The Astrophysical Journal, 617:1–28, 2004 December 10

COSMOLOGICAL PARAMETERS σ_8, THE BARYON DENSITY Ω_b, THE VACUUM ENERGY DENSITY Ω_Λ, THE HUBBLE CONSTANT AND THE UV BACKGROUND INTENSITY FROM A CALIBRATED MEASUREMENT OF H I Lyα ABSORPTION AT $z = 1.9$[1]

David Tytler, David Kirkman, John M. O'Meara, Nao Suzuki, Adam Orin, Dan Lubin, Pascal Paschos, Tridivesh Jena, Wen-Ching Lin, and Michael L. Norman
Center for Astrophysics and Space Sciences, University of California, San Diego;
MS 0424, La Jolla; CA 92093-0424; tytler@ucsd.edu

and

Avery Meiksin
Institute for Astronomy, Edinburgh, Blackford Hill, Edinburgh EH9 3HJ, UK
Received 2004 March 30; accepted 2004 July 22

ABSTRACT

We identify a concordant model for the intergalactic medium (IGM) at redshift $z = 1.9$ that uses popular values for cosmological and astrophysical parameters and accounts for all baryons with an uncertainty of 5%. The amount of absorption by H I in the IGM provides the best evidence on the physical conditions in the IGM, especially the combination of the mean gas density, the density fluctuations, the intensity of the ionizing flux, and the level of ionization. We have measured the amount of absorption, known as the flux decrement (DA), in the Lyα forest at redshift 1.9. We used spectra of 77 QSOs that we obtained with 250 km s^{-1} resolution from the Kast spectrograph on the Lick observatory 3 m telescope. We fitted unabsorbed continua to these spectra using *b*-splines. We also fitted equivalent continua to 77 artificial spectra that we made to match the real spectra in most obvious ways: redshift, resolution, signal-to-noise ratio (S/N), emission lines and absorption lines. The typical relative error in our continuum fits to the artificial spectra is 3.5%. Averaged over all 77 QSOs, the mean level is within 1%–2% of the correct value, except at S/N < 6, where we systematically placed the continuum too high. We then adjusted the continua on the real spectra to remove this bias as a function of S/N and a second smaller bias. Absorption from all lines in the Lyα forest at $z = 1.9$ removes DA($z = 1.9$) $= 15.1\% \pm 0.7\%$ of the flux at rest-frame wavelengths $1070 < \lambda_r < 1170$ Å. This is the first measurement using many QSOs at this z, and the first calibrated measurement at any redshift. Using similar methods on $1225 < \lambda_r < 1500$ Å, we find metal lines absorb an average 1.6% the flux, increasing slightly as the rest-frame wavelength λ_r decreases because more types of spectral lines contribute and there is more C IV at lower redshifts. We estimate that the metal lines absorb $2.3\% \pm 0.5\%$ of the flux in the Lyα forest at $z = 1.9$. The absorption from Lyα alone then has DA $= 12.8\% \pm 0.9\%$. The Lyα lines of Lyman limit systems with H I column densities $\log N_{\rm H\,I} > 17.2$ cm^{-2} are responsible for a DA $= 1.0\% \pm 0.4\%$ at $z = 1.9$. These lines arise in higher density regions than the bulk of the IGM Lyα absorption, and hence they are harder to simulate in the huge boxes required to represent the large-scale variations in the IGM. If we subtract these lines, for comparison with simulations of the lower density bulk of the IGM, we are left with DA $= 11.8\% \pm 1.0\%$. The mean DA in segments of individual spectra with $\Delta z = 0.1$, or 153 Mpc comoving at $z = 1.9$, has a large dispersion, $\sigma = 6.1\% \pm 0.3\%$ including Lyman limit systems (LLSs) and metal lines, and $\sigma(\Delta z = 0.1) = 3.9^{+0.5}_{-0.7}\%$ for the Lyα from the lower density IGM alone, excluding LLSs and metal lines. This is consistent with the usual description of large-scale structure and accounts for the large variations from QSO to QSO. Although the absorption at $z = 1.9$ is mostly from the lower density IGM, the Lyα of LLSs and the metal lines are both major contributors to the variation in the mean flux on 153 Mpc scales at $z = 1.9$, and they make the flux field significantly different from a random Gaussian field with an enhanced probability of a large amount of absorption. We find that a hydrodynamic simulation on a 1024^3 grid in a 75.7 Mpc box reproduces the observed DA from the low-density IGM alone when we use popular parameters values $H_0 = 71$ km s^{-1} Mpc^{-1}, $\Omega_b = 0.044$, $\Omega_m = 0.27$, $\Omega_\Lambda = 0.73$, $\sigma_8 = 0.9$, and an ultraviolet background (UVB) that has an ionization rate per H I atom of $\Gamma_{912} = (1.44 \pm 0.11) \times 10^{-12}$ s^{-1}. This is 1.08 ± 0.08 times the prediction by Madau et al. with 61% from QSOs and 39% from stars. Our measurement of the DA gives a new joint constraint on these parameters, and the DA is very sensitive to each parameter. Given fixed values for all other parameters, and assuming the simulation has insignificant errors, the error of our DA measurement gives an error on H_0 of 10%, Ω_Λ of 6%, Ω_b of 5%, and σ_8 of 4%, comparable to the best measurements by other methods.

Subject headings: cosmological parameters — cosmology: observations — diffuse radiation — methods: data analysis — quasars: absorption lines — techniques: spectroscopic

[1] Based on data obtained with the Kast spectrograph on the Lick Observatory 3 m Shane Telescope.

1. INTRODUCTION

Our physical understanding of the intergalactic medium (IGM) comes from the detailed comparison of numerical simulations of the growth of structure in the universe with observations of the Lyα absorption from the H I in the IGM. Analytic models show that the amount of Lyα absorption depends on a combination of at least four factors: the mean density of H in the IGM, the power spectrum of the matter distribution that determines the amount of clumping of the H on various scales, the temperature of the gas, and especially the mean intensity of the UVB radiation that photofinishes the gas. Together, these parameters and their variation give the density of H I down the line of sight to a QSO, something we observe with Lyα absorption.

The mean amount of absorption is a sensitive measure of the physical properties of the IGM. If we make some assumptions about the growth of structure and the temperature of the IGM, then the optical depth of the Lyα forest scales as (Rauch et al. 1997, eq. [17])

$$\tau_{\rm Ly\alpha} \propto (1+z)^6 H(z)^{-1} (\Omega_b h^2)^2 T^{-0.7} (\rho/\overline{\rho})^2 \Gamma_{912}^{-1}, \qquad (1)$$

where ρ is the baryon density, $\overline{\rho}$ is the mean baryon density, Γ_{912} is the photoionization rate per H I atom, and T is the gas temperature. The parameters are not independent, since, for example, lower temperatures are expected for lower Ω_b (Theuns et al. 1999; Gardner et al. 2003). At $z = 2$ lower density gas is typically cooler, and there is a range of temperatures for a given density, especially at higher z in more realistic treatments with radiative transfer that ionize different volumes at different times (Bolton et al. 2004; Hui & Haiman 2003). However, to first order, the amount of Lyα absorption at some wavelength in a spectrum reflects the density of H I in part of the IGM, and this is closely related to the density of the gas and dark matter.

Many authors have to used this relationship, together with an estimate of Γ_{912}, to estimate the cosmological baryon density from the mean amount of absorption in the Lyα forest. The $\Omega_b h^2$ estimates have all been too large (Haehnelt et al. 2001, Fig. 4). Rauch et al. (1997, eq. [8]) estimated $\Gamma_{912} > 7 \times 10^{-13}$ s^{-1} at $z = 2$ because of the contribution to the UVB from known QSOs, which is consistent with the $\Gamma_{912} = 8.15 \times 10^{-13}$ s^{-1} due to QSOs from Haardt & Madau (1996). This corresponds to $\Omega_b h^2 > 0.021$ in a ΛCDM model. Steidel et al. (2001) found that a large fraction of ionizing photons escape from Lyman break galaxies, giving $\Gamma_{912} > 1.5 \times 10^{-12}$ s^{-1}. Haehnelt et al. (2001) used this to conclude $\Omega_b h^2 > 0.06$ in their ΛCDM models, while Hui et al. (2002) assumed different mean temperature for the IGM and found $\Omega_b h^2 = 0.045 \pm 0.008$. These values are higher than the more robust measurements of $\Omega_b h^2 = 0.021 \pm 0.002$ from our measurements of D/H using standard big bang nucleosynthesis (Kirkman et al. 2003), and $\Omega_b h^2 = 0.0224 \pm 0.0009$ from the anisotropy of the cosmic microwave background (CMB; Spergel et al. 2003). In this paper we present a more accurate measurement of the mean amount of absorption in the Lyα forest, DA, and for the first time we find that this is consistent with $\Omega_b = 0.044$ in a popular cosmological model.

An accurate measurement of DA is also a critical input to the measurement of the power spectrum of matter using the Lyα forest (Croft et al. 2002b). This is because a smaller DA value requires a larger amplitude for the matter power spectrum if all other factors are unchanged. The larger the matter power amplitude, the less gas is left widely distributed in the IGM where it causes the most absorption. For a given simulation, the DA determines the relationship between the mass field and the Lyα forest optical depth—which we use to infer the Lyα forest mass power spectrum from the Lyα forest flux power spectrum. Hence, the DA can be used to fix the constant of proportionality in equation (1) above. The DA also has an effect on the shape of the power spectrum deduced from the Lyα forest (Zaldarriaga et al. 2003; Seljak et al., 2003, Fig. 1*b*).

Whether the power spectrum measured by the Lyα forest might have lower amplitude than that expected from measurements on larger scales from galaxies and the CMB (Spergel et al. 2003) depends upon the accuracy of the Lyα forest DA measurements. Croft et al. (2002b) stressed that the uncertainty in the DA is the main source of error in estimates of the matter power spectrum from the Lyα forest. Their Figure 17 shows how the amplitude of the matter power spectrum changes with the mean opacity, for a fixed flux power. They chose $\tau_{\rm eff}(z = 2.72) = 0.349$ from Press et al. (1993, hereafter PRS93). If instead we now choose $\tau_{\rm eff}(z = 2.72) = 0.280$, from the right-hand side of Figure 1 of Schaye et al. (2003), which we expect is more accurate, the Croft et al. (2002b) results show that the matter power spectrum rises by a factor of 2.1, assuming no change to the temperature-density relation in the IGM. Seljak et al. (2003) also discussed this situation in detail. They reviewed DA estimates and chose $\tau_{\rm eff}(z = 2.72) = 0.298$, from McDonald et al. (2000). They too find that this change increases the matter power by a factor of 2 compared to the value in Croft et al. (2002b) when combined with an increase in the slope of the matter power spectrum.

Croft et al. (2002b, eq. [12]) find that the three-dimensional matter power spectrum amplitude $\propto \tau_{\rm eff}^{-3.4}$, for a given observed flux power. This implies that to measure the power spectrum amplitude to 10% at $z = 2.72$, we would need a relative error on $\tau_{\rm eff} = 0.298$ of 3%, which is a relative error on DA = 25.8% of 2.5% and an absolute error on DA of 0.7%, assuming that all other factors were well known, which is not the case. We find a similar scaling relation from Seljak et al. (2003).

However, Gnedin & Hamilton (2002, eq. [8]) find a much weaker correlation between the matter power and the DA. Although the origin of this disagreement is unknown, Seljak et al. (2003) suggest that Gnedin & Hamilton (2002) did not sample a wide enough range of parameters. Larger amplitude power comes with higher velocities, which decreases the flux power on small scales. As the matter power increases, the flux power can both rise on large scales and fall on small scales.

Recently Viel et al. (2004, Fig. 4 and eq. [5]) report a result intermediate between Croft et al. (2002b) and Gnedin & Hamilton (2002): the three-dimensional matter power spectrum amplitude $\propto \tau_{\rm eff}^{-1.4}$.

These results show that high-accuracy DA measurements are of great interest because of their cosmological significance. In general, accurate measurements of DA can become a cornerstone in a concordance model of the IGM, tying together the intensity of the UVB, the thermal history of the IGM, and the cosmological matter power spectrum.

1.1. *Definition of DA*

Following Oke & Korycansky (1982), we define DA = $1 - \langle F \rangle$, where $\langle F \rangle$ = (observed flux)/C, and, C = (estimated unabsorbed continuum flux), which includes both the underlying power law and the flux from emission lines. It is common to see DA expressed as $\langle F \rangle$, or as the mean effective optical depth, $\tau_{\rm eff} = -\ln \langle F \rangle$.

We measure DA in individual pixels, and we add suffixes to DA to label averages over various wavelengths between the Lyα and Lyβ emission lines, sometimes averaged over many QSOs. We restrict our measurement of DA to rest-frame wavelengths

$$\text{DA wavelength range} = 1070\text{–}1170 \text{ Å}. \quad (2)$$

The DA is dominated by Lyα lines from the IGM, but it includes all absorption, including metal lines and the Lyα lines from Lyman limit systems (LLSs) that are defined to have H I column densities $\log N_{\rm H\,I} > 17.2$ cm^{-2}. The LLSs by definition include all damped Lyα lines (DLAs) that have $N_{\rm H\,I} > 2 \times 10^{20}$ cm^{-2}.

After we measure the DA, we give estimates for the amount of absorption due to the Lyα lines of high column density absorption systems and metal lines, both of which are harder to simulate.

1.2. *Prior Measurements of DA*

More than a dozen papers contain measurements of DA (see references in Rauch [1998] and Bernardi et al. [2003, hereafter B03] and the discussion of errors in Croft et al. [2002b] and Seljak et al. [2003]).

The DA is hard to measure because we need many QSO spectra, the unabsorbed continuum level is hard to estimate, and when we want just the H I portion of the DA, the metal lines in the Lyα forest are difficult to find and measure.

To measure the mean DA with a relative error of 1%, i.e., DA $= 0.300 \pm 0.003$, in a specific redshift range, we must observe about 10,000 Lyα lines with $N_{\rm H\,I}$ values similar to those that make most of the optical depth (Kirkman & Tytler 1997, Fig. 8). We need on the order of 100 QSOs at $z = 3$. Most samples have used under 10 QSOs.

The unabsorbed continuum is relatively easy to find in high-resolution spectra with high signal-to-noise ratios (S/Ns), but we have few of these spectra. Instead, the continuum in the Lyα forest has often been set to a power law extrapolated from wavelengths greater than 1250 Å, and this can be biased (Kim et al. 2001, hereafter KCD01; Meiksin et al. 2001; Seljak et al. 2003).

Most papers have not attempted to find and remove metal lines. Instead they include such lines in their DA values.

These difficulties have led to large differences in reported DA values. Jenkins & Ostriker (1991) noted that the distribution of flux in the Lyα forest region implies that there is about 30% more absorption than is expected from lines identified in spectra, which is a huge uncertainty. For example, at $z \simeq 3$ we have $\tau_{\rm eff} = 0.28$, 0.38, and 0.45 from Hu et al. (1995), Rauch et al. (1997), and PRS93, respectively, while at $z = 2.72$ we have $\tau_{\rm eff} = 0.28$ from Schaye et al. (2003) and 0.35 from both PRS93 and B03.

The uncertainty over the DA has hindered attempts to measure parameters such as Ω_b from the Lyα forest. Zhang et al. (1998) obtained the DA from a conventional power-law fit to the $N_{\rm H\,I}$ distribution by Hu et al. (1995), who in turn had used Keck spectra of four QSOs all at $z = 3.1$–3.4. We know that the integral over this power law could contain large errors. Weinberg et al. (1997) used PRS93 very low resolution (25 Å) spectra of 29 QSOs at $z = 2.5$–4.3. We discuss the most detailed study, by Rauch et al. (1997), later.

Two recent measurements of the DA are of special interest. B03 used 1061 Sloan Digital Sky Survey spectra to measure the DA at $2.6 < z_{\rm abs} < 4.0$, again at higher redshifts than the spectra we use. They introduce new methods and obtain by far the best random error, although there seem to be systematic problems with their results. Schaye et al. (2003) used 21 UVES and HIRES spectra, with S/N > 40, and they removed metal lines. They found $\tau_{\rm eff}$ values that are systematically lower than those of B03 by 0.1 dex.

Recently, Meiksin & White (2004 [hereafter MW04], Table B1) showed that some of the disagreement in the DA values has come from the conversion from $\tau_{\rm eff}$ to DA. Correcting for this, they find that measurements at low resolution (PRS93), intermediate resolution (Steidel & Sargent 1987, hereafter SS87), and high resolution KCD01 agree at $z = 2.41$–4.0. However, the (B03) DA values are larger than others across this z range.

1.3. *What We Do*

We make artificial spectra with similar characteristics to the Kast spectra set (e.g. S/N, resolution, redshift, and continuum shape). We fit continua to these spectra, and we measure and use the errors in these continua to correct the continua on the Kast spectra. We aim for an absolute error in the mean DA value at $z = 1.9$ of less than 1%, dominated by the random noise coming from the sample size. This correspondS to a relative error of less than 6.6% on the total DA value and less than 8.5% when the total excludes metal lines and the Lyα of LLSs.

The paper is organized as follows. In §§ 2–5 we describe our data set and calibration methods. In § 2 we describe the Kast spectra; in § 3 we describe the artificial spectra that we create to calibrate the continuum fit; in § 4 we describe the continuum fits; and in § 5 we measure and correct the errors we made in the continuum fits.

We describe the results of our DA measurement starting in § 6. In § 9 we describe the dispersion we see in the DA, and in § 11.2 we measure and summarize the error on the DA. In § 12 we present hydrodynamic simulations and deduce cosmological parameters. In §§ 11.1 and 13 we show how the error changes with sample size. In § 15 we summarize and discuss our results.

In Table 1 we collect the definitions of the new terms that we use to track various measurements. To convert from redshift to distance, we use a Hubble constant $H_0 = 71$ km s^{-1} Mpc^{-1}, a vacuum energy of $\Omega_\Lambda = 0.73$, and a matter density of $\Omega_m = 0.27$, and we evaluate at $z = 1.9$.

2. KAST QSO SPECTRA

We obtained spectra of the Lyα forest of over 80 bright QSOs at $1.85 < z_{\rm em} < 2.5$. We maintained a list of all such QSOs listed in NED and updated it before each observing run. We found about 6000 QSOs of all magnitudes. We rejected those noted as BAL (broad absorption lines) in NED, and we then observed the brightest remaining at declination north of $-30°$. Most were 17th magnitude. We observed nearly all that were brighter than 17.5 and some that were 18th magnitude. We rejected BAL QSOs because they tend to show much more absorption than other QSOs. In the Lyα forest region this absorption is from N V and other ions. BAL QSOs would also bias our estimates of the mean amount of metal line absorption because they can have huge amounts of C IV and Si IV absorption.

2.1. *Observations*

We obtained spectra from 2001 January 26 to 2003 July 28 with the Kast double spectrograph on the Shane 3 m telescope

TABLE 1
Definitions of Terms

Term	Definition
DA range	We measure DA at rest-frame wavelengths 1070–1170 Å
DA	Amount of absorption from all lines, including LLSs, DLAs, and metals
DA0	DA measured pixel by pixel
DA1	Mean DA measured in segments 4.5 Å rest in size
DA2	Mean DA from a single QSO in a redshift range of $\Delta z = 0.1$
DA2*s*	DA2 at $z = 1.900$ after each pixel corrected for the $(1 + z)$ trend, using eq. (5)
DA3	DA in quarters of our sample
DA4	Mean DA measured between 1070 and 1170 Å rest
DA4*s*	DA4 after each pixel corrected for the $(1 + z)$ trend, using eq. (5)
DA5	Analytic equation for DA from counted Lyα lines
DA6*s*	Absorption by the Lyα lines of LLSs, including DLAs, at $z = 1.9$
DA7*s*	DA4*s* − DM*s*
DA8*s*	DA4*s* − DA6*s* − DM*s*
DM	Amount of absorption from metal lines alone
DM1(λ_r)	Fit to DM in Kast spectra as function of rest wavelength, using eq. (9)
DM2(λ_o)	Fit to DM in Kast spectra as function of observed wavelength, using eq. (10)
DM3(λ)	The mean DM from a segment of the spectrum of one QSO that is 121.567 Å wide in the observed frame, corresponding to $\Delta z = 0.1$ for Lyα
DM4(λ)	Absorption from lines with known equivalent widths, using eq. (11)
DM5(λ_r)	Fit to DM4 from SBS88 as function of rest wavelength, using eq. (12)
DM6(λ_o)	Fit to DM4 from SBS88 as function of observed wavelength, using eq. (13)
DM7(1548)	DM from the C IV line at 1548 Å, from SBS88, using eq. (14)
DM7(C IV)	DM from both C IV lines, from SBS88, using eq. (15)
DM*s*	Amount of absorption by metal lines in DA region 1070–1170 Å
γ_{912}	Photoionization rate per H I atom in the low-density optically thin IGM, in units of the predicted rate at $z = 1.9$ from Madau et al. (1999)
γ_{228}	As γ_{912}, but for He II
SDA	DA smoothed using an exponential filter with FWHM 25 Å rest
SNR	Usual S/N pixel^{-1}
SNR2	Indicator of the data quality on a large scale, representing the smoother S/N that we would have measured in absence of absorption and emission lines
F1/TC	(fitted continuum, raw)/(true continuum) ratio
F2/TC	(fitted continuum, corrected with SNR2)/(true continuum) ratio
F3/TC	(fitted continuum, corrected with SNR2 and SDA)/(true continuum) ratio

at Lick observatory. We present the observing log and spectra in Tytler et al. (2004). Here we use spectra obtained with the blue camera, using the grism with 830 groves mm^{-1}, blazed at 3460 Å, and covering approximately 3150–4300 Å.

We know from prior work with this instrument (Suzuki et al. 2003) that the typical dispersion is 1.13 Å pixel^{-1} (107 km s^{-1}), and the FWHM resolution is 250 km s^{-1} (2.5 pixels), with a range of 200–300 km s^{-1}, depending on the temperature and the focus that we chose for that observing run. The spectral resolution varies with wavelength and from run to run, even when the slit is unchanged. We describe the data reduction and flux calibration in Tytler et al. (2004).

We changed the flux in the occasional pixel, under 1% of all pixels, that was clearly erroneous because of poor cosmic-ray or sky subtraction. We set such pixels to the expected level, to reduce the effect on the continuum fitting and the DA estimate. Hence the spectra are cosmetically unusually clean.

2.2. *QSO Sample Used*

We attempted to set the integration times to reach S/N = 10 per pixel at 3200 Å, although weather sometimes prevented us from achieving this. The S/N in the continuum of the spectra from Lyβ to Lyα varies from a few to over 50, with typical values of 6–20. Some of this variation is from QSO to QSO, at a given wavelength, and some is variation with wavelength within each spectrum. For all spectra, the S/N increases systematically with wavelength, and hence with z_{abs}. This has important consequences that we discuss below. We show the S/N with the spectra and list values at rest wavelengths 1070 and 1170 Å in Tytler et al. (2004, Table 2).

We reject about 10 QSOs because the S/N was less than 2, and we reject Q2310+0018 (R.A. = $23^h10^m50^s.80$, decl. = $+00^\circ18'26''.4$ (B1950), $z_{em} = 2.200$ mag. 17.00) because we discovered that it shows BAL absorption. We are left with Lyα forest spectra of 77 QSOs that we use in this paper. In addition to Q2310+0018, Tytler et al. (2004) also includes spectra of a second BAL QSO, Q1542+5408, that we do not use in this paper.

We measured the z_{em} for each QSO from the emission lines in its blue spectrum, typically Lyα and Si IV and sometimes Lyβ–O VI and C IV. We list the QSO names and these z_{em} values in Tytler et al. (2004), Table 1.

In Figure 1 we show a histogram of the z_{em} values, and the number QSOs contributing Lyα forest information at various z_{abs} values. The mean $z_{em} = 2.17$, while the mean $z_{abs} = 1.924$ for wavelengths in the DA range. Had we weighted by S/N, the mean z_{abs} would have been greater than 2. We use spectra with observed wavelengths 3173–4083 Å with a range of ±5 Å from the precise CCD placement. This corresponds to $z_{abs} = 1.6105-2.3587$ for Lyα. Eight of the QSOs with $z_{em} < 1.965$ do not cover the whole 1070–1170 Å range, since their 1070 is less than 3173 Å.

When we use the entire sample to measure the DA, which we call DA4, we sample a total redshift path of 19.750 (30.8 comoving Gpc) in 23,000 pixels of 1.13 Å in the observed frame.

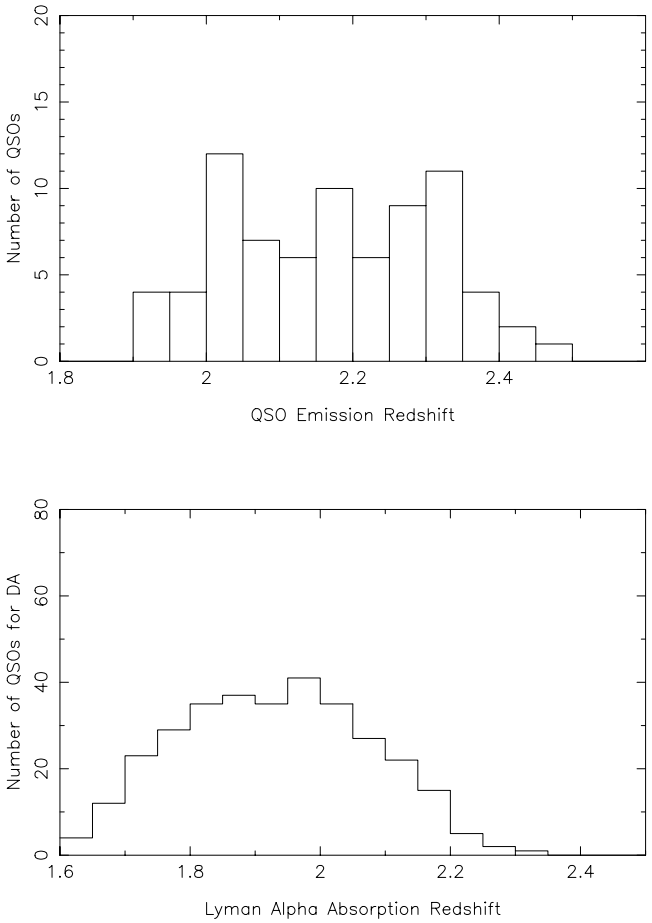

FIG. 1.—*Top:* Nmber of QSOs in our sample as a function of emission redshift. *Bottom:* Nmber of QSOs that contribute to our measurement of the DA at each redshift.

At a redshift of 1.9, one pixel corresponds to 1.45 comoving Mpc, for a model with $H_0 = 71$ km s^{-1} Mpc^{-1}, $\Omega_\Lambda = 0.73$, and $\Omega_m = 0.27$.

3. ARTIFICIAL QSO SPECTRA

We have made a set of 77 artificial spectra, each one matched to one of the Kast spectra. Each artificial spectrum has the same $z_{\rm em}$ and S/N distribution as one of the Kast spectra. All the artificial spectra have shapes, including emission lines, from real *Hubble Space Telescope* (*HST*) spectra of lower redshift QSOs; they all have random Lyα absorption lines; and they have the same spectral resolution as the Kast spectra.

The starting point for the artificial spectra were the smoothed absorption free fits to the continuum and emission lines of the 50 QSOs discussed and listed in Table 1 of Suzuki et al. (2004). They have $0.14 < z_{\rm em} < 1.04$ and an average S/N = 19.5 per 0.5 Å in the rest frame from 1050–1170 Å. The *HST* continua on these spectra had previously been adjusted to match our understanding of QSO continua. We believe that the continua levels are better known than those for the Kast spectra, because the S/N is relatively high and there are far fewer absorption lines at these low redshifts. In a quick look, the shapes of these *HST* spectra are not obviously different from those of the QSOs that we observed with the Kast spectrograph.

We randomly associated each of the *HST* spectra with one of the Kast spectra, and we use 27 of the *HST* spectra twice. These associations match each of the $z_{\rm em}$ values to one and only one of the artificial spectra. We trimmed the wavelength range of each artificial spectrum to match the range of its paired Kast spectrum.

Next, we added Lyα absorption from heuristic simulations of the Lyα forest. The model used for the forest is a simplified version of the Bi et al. (1992) lognormal model, which incorporates nonlinear effects into the linear theory of structure formation. In the lognormal model, the transmission fraction field is simply defined to be

$$F(\lambda) = \exp\left\{-\tau_0 \exp\left[\delta(\lambda) - \sigma^2/2\right]^2\right\}\left\{-\tau_0 \exp\left[\delta(\lambda) - \sigma^2/2\right]^2\right\}, \quad (3)$$

where $\delta(\lambda)$ is a Gaussian random field. The power spectrum of δ, $P_\delta(k)$, was constructed to make the simulated power spectrum of F, $P_F(k)$, roughly match the observed $P_F(k)$ (e.g., from McDonald et al. 2000). We made $\tau_0(z)$ and the amplitude of $P_\delta(k, z)$ slowly varying functions of redshift to match observations. The change in the total absorption due to Lyα in these simulated spectra should follow $A(1+z)^\gamma$, where $A = 0.0166$ and $\gamma = 2.07$. The simulations were made with full numerical resolution, and then smoothed to a FWHM of 250 km s^{-1}.

We added the absorption starting at 1215.67 Å (rest frame, as are the rest of the wavelengths in this section). This is typically near the peak of the Lyα emission line using the $z_{\rm em}$ value that we had measured. The absorption was added by multiplying the smoothly changing fit to the *HST* spectrum by flux values from 0–1. We continued the absorption down to the UV end of the spectrum. The spectra contain only Lyα absorption, even when we are at wavelengths where Lyβ would also appear in Kast spectra. We did not make any adjustments for the proximity effect, and hence the absorption from the Lyα forest in the artificial spectra begins at exactly 1215.67 Å.

These simulations produce Lyα forest absorption that is similar to Kast spectra, but they were not adjusted to be as close as possible. Compared to Kast spectra, the simulations have too few Lyα with large equivalent widths coming from the LLSs, and they have no DLAs. Otherwise, by visual inspection alone, we cannot tell the artificial spectra from the real Lyα forest. The lack of a proximity effect region is not a distinction, since this can not be seen in a single spectrum.

We added a Gaussian random deviate to each pixel in each artificial spectrum to make its S/N similar to that of its partner. This procedure is complicated because we wish to simulate the S/N that we would have obtained with Kast had we observed the QSO with the $z_{\rm em}$ of its partner and the spectral slope and emission lines of the *HST* spectrum. Hence, we cannot simply copy the S/N from the Kast spectrum partners, because the emission and absorption lines differ.

The S/N that we gave to an artificial spectrum had the same values as the S/N in its partner spectrum at two reference wavelengths, 1100 and 1255 Å, and it responds to emission and absorption lines according to the (flux)$^{1/2}$ in the artificial spectrum.

In detail we multiplied the flux in each artificial spectrum by the response function of the Kast, to simulate the distribution of photons that we would have recorded had we observed the *HST* flux distribution. The square root of this gives the relative S/N as a function of wavelength. We then measured the S/N in both the artificial and Kast spectra averaging over 0.02 in z (24.3 Å rest) around each reference wavelength. We took the ratios of these S/N values, Kast upon artificial, to derive

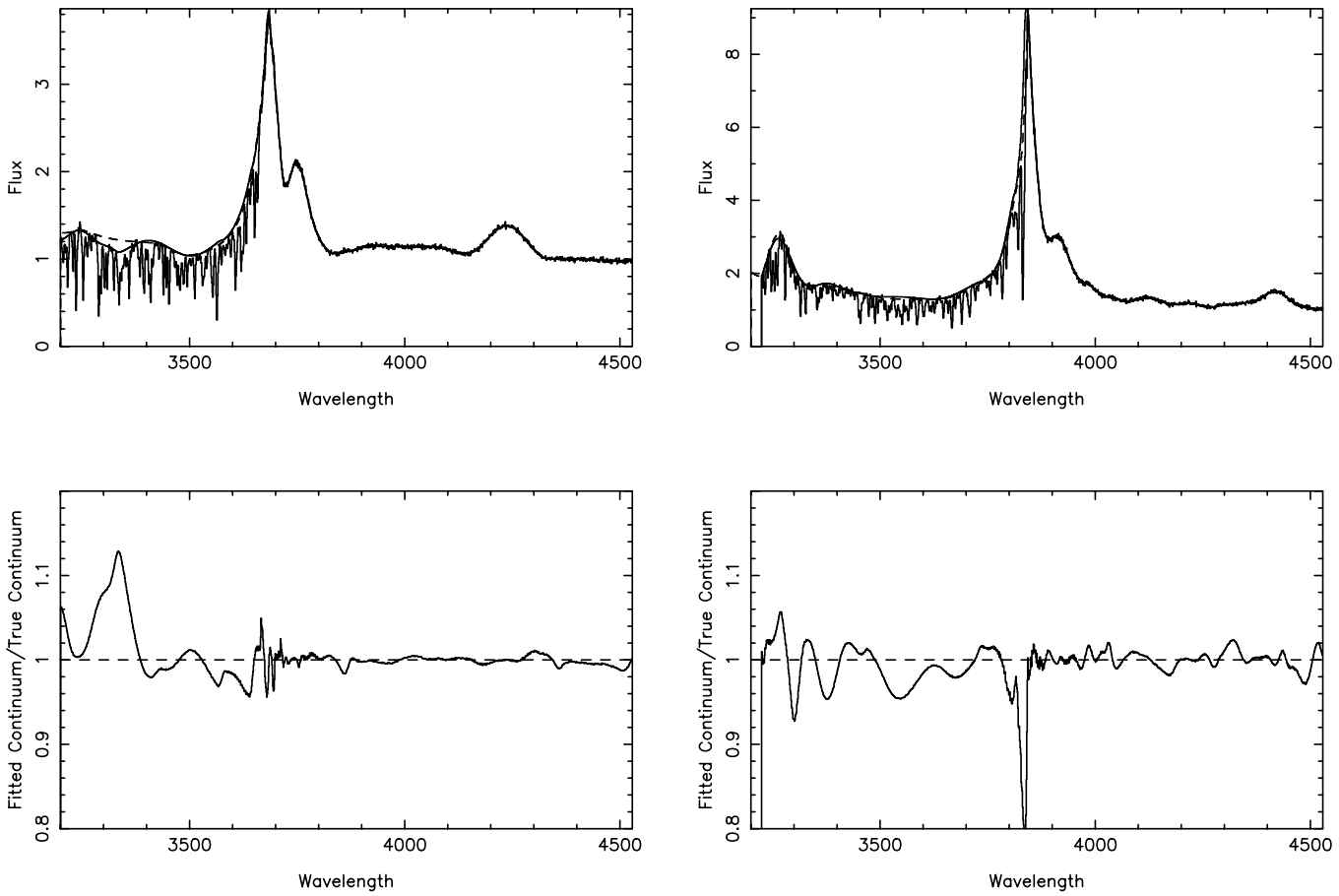

FIG. 2.—Examples of the continua that we fitted two artificial QSO spectra. In the top panel for each QSO the solid curve is the true continuum and the dashed line our fit. Under each spectrum we show the fitted continuum divided by the true continuum: F1/TC. The spectrum on the left has the largest error in the Lyα forest of any spectrum with high S/N. The artificial spectrum on the right was selected at random and also happens to have high S/N.

correction factors. We fitted a straight line between the two correction factors and then multiplied the S/N on the artificial spectrum by this line. The artificial and Kast spectrum then have the same S/N at the reference wavelengths and generally similar distributions of S/N with wavelength. We checked that the distribution of S/N in the DA region in the 77 artificial spectra was very similar to that in the 77 Kast spectra.

In Figure 2 we show two artificial spectra. The only easy way to see that these are artificial is that there is zero absorption redward of Lyα.

4. CONTINUUM FITTING

The methods that have been used to estimate the unabsorbed continuum in the Lyα forest fall into two general classes:

1. Extrapolations from wavelengths greater than 1250 Å (rest frame, as are the other wavelengths in this section) that do not use the flux information from the Lyα forest. The extrapolations use power laws (Oke & Korycansky 1982; SS87; B03), similar smooth functions (PRS93), or principal components that also predict the shapes of emission lines in the Lyα forest (Suzuki et al. 2004).
2. Fits to the local continuum in the Lyα forest that emphasize the wavelengths with the most flux (Rauch et al. 1997; Fang et al. 1998; McDonald et al. 2000; Kim et al. 2002; Schaye et al. 2003).

The values that we quoted in § 1 illustrate that the extrapolations give systematically much more DA than do fits to the local continuum, a point noted by others (KCD01; Meiksin et al. 2001; Seljak et al. 2003). Like other authors, we suspect that the extrapolated continua are less reliable and too high in the Lyα forest.

Seljak et al. (2003) suggest that the extrapolated continuum is too high because QSO spectra are not well fitted by a power law with a single slope. It is well established that the best-fit power law declines faster with decreasing wavelength at less than 1200 than at greater than 1300 Å (Telfer et al. 2002, Fig. 4). Seljak et al. (2003) calculate that the DA from power-law extrapolations should be decreased by at least 0.05 to correct this bias. The precise correction will depend on how and where the power-law fit was made to the spectra, since there are many strong blended emission lines at greater than 1250 Å.

A second reason why the extrapolations might be biased is that the shape of the typical QSO spectrum in the Lyα forest is much more complex than a pair of power laws. Figure 5 of PRS93, Figure 6 of Vanden Berk et al. (2001), Figures 4 and 9 of Telfer et al. (2002), Figure 3 of B03, and Figures 2 and 3 of Suzuki et al. (2004) all clearly show that the region from Lyβ–O VI to Lyα is dominated by the wings of those two emission lines, and by lines near 1073 Å (possibly a blend of S IV, He II, N II and Ar I, according to Scott et al. [2004], or He II, N II and Fe II, according to Telfer et al. [2002], or Ar I, according to Zheng et al. [1997]) and 1123 Å (Fe III). In some spectra 1073 and 1123 are weak, but in the mean spectrum they are strong enough that all wavelengths are influenced by one or more of these four lines, separated by three flux minima, near 1050,

1100, and 1150 Å. The flux minimum near 1050 Å between Lyβ and 1073 Å is especially hard to recognize in spectra with a lot of absorption or low S/N, and although we were looking for it, in some cases we missed it, as in the left panel of Figure 2.

There are also weaker emission lines near 1176 Å (C III*; Vanden Berk et al. 2001; Telfer et al. 2002; Suzuki et al. 2004), and possibly 1195 (Si II; Telfer et al. 2002) and 1206 Å (Si III; our HIRES spectrum) all in the wings of the Lyα line, and outside our DA region.

In Tytler et al. (2004) we list the wavelengths of the emission lines in the Kast spectra of the QSOs. We find that three strongest emission lines, or line blends, between Lyβ and Lyα have mean rest wavelengths of 1070.95 ± 1.00, 1123.13 ± 0.51, and 1175.88 ± 0.30 Å.

The sign of the bias in the continuum that comes from ignoring these lines will depend on the details of the continuum extrapolation or fit, and in the case of a fit, on whether the person making the local continuum fit was aware of these lines, attempted to fit them, and had spectra of wavelengths greater than 1216 Å where other emission lines suggest the likely strengths of the Lyα forest lines.

B03 were the first to call attention to the emission lines near 1073 and 1123 Å, and they fitted QSO continua with power law plus three Gaussian functions, one each for these lines and Lyα.

In Suzuki et al. (2004) we used principal component analysis to predict the shape of the Lyα forest continuum and emission lines in individual spectra, using the shape of the spectrum at wavelengths 1216–1600 Å. The results were sometimes excellent, but other times poor, in part because of the sensitivity to the flux calibration. The predicted flux in the Lyα forest of a QSO had an average absolute error of 9%, with a range from 3%–39%, which is too large an error for a DA measurement, especially since we do not know whether the mean is systematically too high or too low.

Among the methods that use the local flux in the Lyα forest we note Fang et al. (1998), who used the mode of the distribution of flux to estimate the continuum level on our HIRES spectrum of one bright QSO. This works best when the S/N is very high and the spectral resolution is high enough to show regions with minimal absorption, neither of which is the case for our Kast spectra.

4.1. *The Local Continuum Fits That We Made*

The method that we use to fit continua is that often used on high-resolution spectra with high S/N: fitting a different smooth curve to each Lyα forest spectrum. This method is routinely used for measurements of absorption lines and for the DA when the spectra have high resolution, high S/N, and the $z_{\rm abs}$ is low enough that there are some regions that appear to be absorption free.

Rauch et al. (1997) fitted local continua to Keck HIRES spectra of seven QSOs at $z_{\rm em} = 2.5-4.6$ that differed widely in S/N. They used spline fit continua with rejection of 3 σ depressions. They corrected their continua upward because some regions lack pixels without absorption. The corrections came from the highest flux in each simulated spectrum, from a box $10\ h^{-1}$ comoving Mpc long for a ΛCDM model. At $z = 2$ this correction was small, from DA = 0.148 to 0.154. We shall also use artificial spectra to make corrections to the whole of each QSO spectrum.

McDonald et al. (2000) fitted local continua to the same spectra used by Rauch et al. (1997) plus one more. They used IRAF to fit Spline3 or Chebyshev polynomials to the continua, which were cut into 2–4 pieces prior to the fits. They fitted to the flux in portions of the spectra that seemed free of absorption, with various orders of polynomial. The fits were complicated because the flux calibration was not good. Schaye et al. (2003) also fitted local continua to 21 UVES and HIRES spectra.

We know from our work on D/H measurement that we can fit the Lyα forest continuum in high S/N HIRES spectra with an error of around 2% (Kirkman et al. 2003). We fitted a smooth curve by eye, using a *b*-spline as a convenient way to store the result. This motivated us to try to use and calibrate the same method on the Kast spectra. We find that the method works because the lower spectral resolution is compensated by the much lower density of Lyα lines at $z \simeq 1.9$, and because we have a large wavelength range, extending to near C IV, in each spectrum.

We used a *b*-spline fit to each spectrum that started with one control point every 50 Å. We added points, especially in the emission lines, and we manually adjusted all points over the entire spectrum to obtain our best guess at the unabsorbed continuum. The continuum is strongly influenced by the observed flux levels throughout a spectrum and by our perception of the strengths and shapes of all the emission lines throughout the spectrum. We did not explicitly assume that any particular part of a spectrum was absorption free.

We paid close attention to the emission lines, especially those at 1073 and 1123 Å (Suzuki et al. 2004). We sorted the spectra according to the strength of these lines, and we attempted to produce a consistent set of lines across the whole of each spectrum, out to C IV. We found that strong lines such as Si II 1263, O I/Si II 1306, and C II 1335 often indicated strong lines near 1073 and 1123.

Two of us reviewed the entire set of fits to the Kast and artificial spectra all in one sitting, to try to make a consistent set of fits for the entire sample. We repeated this exercise after we had made the corrections following the first review.

4.2. *Errors in Our Continuum Fits*

We now examine the errors in the continua that we fit to the artificial spectra. In each case we know the true continuum level. We make the important assumption that the continua on the Kast spectra have similar errors.

To measure the error in our continuum fits, we define

$$\mathrm{F1/TC} = (\text{fitted continuum})/(\text{true continuum}). \quad (4)$$

We measured F1/TC for each pixel in each artificial spectrum. The mean of the absolute fractional error in our continuum fits in the DA region is 3.5%. At a random wavelength in a random QSO, 16% of the pixels have $\mathrm{F1/TC} > 1.051$, and 16% have $\mathrm{F1/TC} < 0.970$. The standard deviation of F1/TC is about 5.4% in the DA wavelength range. At 1216–1500 Å the F1/TC standard deviation is 1.7%.

In Figure 2 we show our F1 continuum fits to two artificial spectra. For each we show both the true and the fitted F1 continuum and the ratio F1/TC. These spectra illustrate several errors typical of the continuum fits. We often underestimate the amount of absorption near the peak of the Lyα line (*right spectrum*). We were aware of this possibility but we still failed to anticipate the full effect. We also failed to give the emission lines enough structure. For the left-hand spectrum we failed to drop down between the Lyβ–O VI blend and the line at 1073 Å, which can be almost as high as Lyβ.

Although the S/N is higher in emission lines, the uncertainty in their shape more than compensates. On average, the

dispersion in F1/TC is slightly larger in the emission lines. In some QSOs the emission lines have typical F1/TC (Fig. 2, *left spectrum*), but in others the Lyα line has the largest continuum error of anywhere in the spectrum (*right spectrum*). Errors are also larger at the UV end of spectra where the S/N is lowest.

We classify our fits around the Lyα emission line peak as follows. For 34 QSOs the fits are good to excellent, and no worse than elsewhere in the Lyα forest. For 31 we fitted too low, usually over a single region 3–10 Å (rest) wide (like the right spectrum in Fig. 2), but sometimes over a wider region. For three QSOs we fitted too high, and for nine we fitted one region too high and another too low. We considered and rejected using this knowledge to adjust our continua on both the artificial and Kast spectra, because it would not change our results.

The errors in the continuum fits were correlated over a variety of lengths, determined by the number of *b*-spline points that we chose to use. We typically could justify using more points where the S/N was high in the Lyα forest, in the red, and where there are many pronounced emission lines. Although there was no particular scale of correlation, we often saw strong correlations over 10–40 Å in the rest frame in the Lyα forest region for most spectra and over a few Å in the Lyα line.

The continua on some of the artificial spectra are poor, with errors of 10%–20%, all across the Lyα forest. Of the four with the largest errors, two have low S/N, but two others have intermediate S/N $\simeq$ 5.

5. CORRECTING THE CONTINUUM LEVELS USING THE ARTIFICIAL SPECTRA

We measured the DA in the DA wavelength range: 1070–1170 Å. We examined plots of our Kast spectra, stacked in rest wavelength, to help us make these choices. We chose these wavelengths to avoid the proximity effect, the wings of Lyα where the continuum is changing rapidly, the Lyβ–O VI blend (1025.72, 1031.9, 1037.6 Å) and the local flux minimum near 1050 Å that is hard to recognize. Associated absorption that was falling toward the QSO at -3000 km s^{-1} (near the maximum velocity ever seen) would have its O VI 1037 at 1048.09 Å. In some spectra the continuum fits get noticeably worse at less than 1070 Å, and we see that the standard deviation increases at less than 1070 Å. For a Lyα line, $\lambda_r = 1170$ Å is 11,300 km s^{-1} or 170 comoving Mpc from a QSOs at the mean $z_{\rm em}$, sufficiently far that we do not expect a significant influence from the observed QSO. Later in this section we see that we systematically fitted the continuum too low in the range 1170–1216 Å.

The mean of the DA values in all pixels in the artificial spectra, averaged over the DA region wavelengths and all artificial spectra, and using the true continua, is 0.1601. This value applies to a mean Lyα $z = 1.924$.

5.1. *Correcting the Continua of the Artificial Spectra Using SNR2*

We defined a new variable, SNR2, to measure the effect of photon noise on the data quality. It is an indicator of the data quality on large scales, and it represents the smoothed S/N that we would have measured in the absence of absorption and emission lines. We ignore both absorption and emission lines because to first order we do not expect our continuum level estimates to be better or worse near a narrow absorption line and we found that the continuum fits are slightly worse in the emission lines.

We defined SNR2 as a smoothly varying function of wavelength, with values similar to the S/N at those wavelengths. It is not smoothed S/N, since this is depressed by absorption lines. Rather it is the flux and S/N in the relatively unabsorbed regions of the spectrum that most influence the continuum fitting accuracy. SNR2 is a linear fit to the S/N values that we measured at the two reference wavelengths.

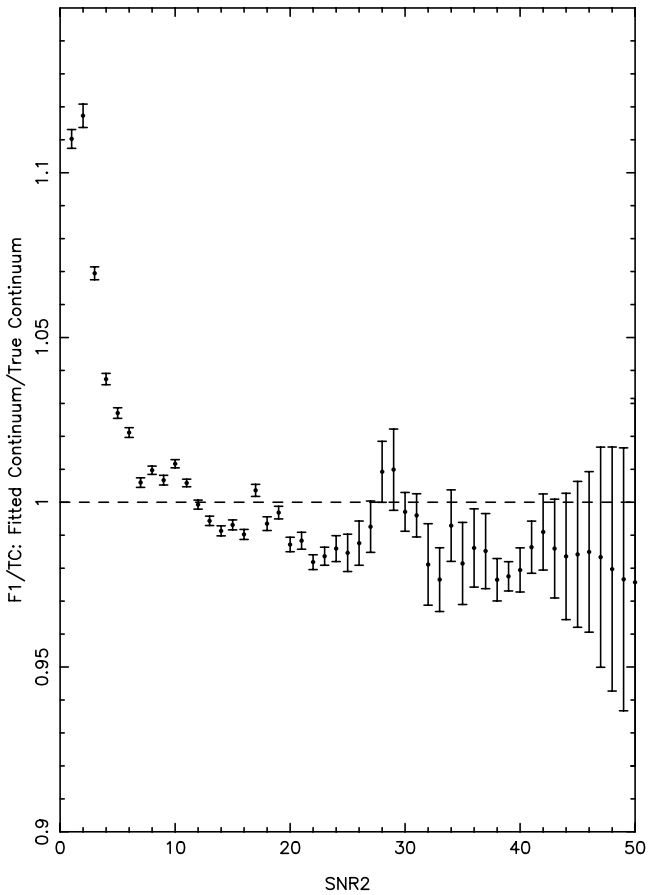

FIG. 3.—Mean fractional error in the continuum level as a function of the data quality, measured by SNR2. The points show the mean ratio of our fitted continuum to the true continuum, F1/TC, in the artificial QSO spectra as a function of SNR2. The error bars on each point indicate the error on the mean value of the fitted/true continuum ratio. The points with the smallest error bars, with SNR2 $\simeq$ 10, are the means that include pixels from the most spectra. The F1/TC values for each pixel have a much larger dispersion, especially for small SNR2.

In Figure 3 we show F1/TC as a function of SNR2. We show the mean F1/TC for all pixels (often over 1000) in a given SNR2 range, and we use all pixels from 1050–1070 Å, which extends to 20 Å lower wavelengths than the DA region. The means show correlation between adjacent bins, since the F1/TC in the spectra are also correlated over tens of Å, and hence over a range in SNR2, which varies smoothly with wavelength. The plot shows that the F1 continua are systematically too high at SNR2 < 6 and usually too low at SNR2 > 12. This type of error is not unexpected.

We made new continua, labeled F2, by dividing the F1 continua on both the Kast and artificial spectra by the factors show in Figure 3.

The correction worked as expected on the artificial spectra. The DA we measured using the initial continua F1 was 0.1687, significantly too large. The DA measured using the F2 continua was 0.1585, which is 0.990 of the value for the input artificial spectra: 0.1601. The DA4(F1) was too large by 5.2%. We checked that when we applied the correction to 1050–1170 Å

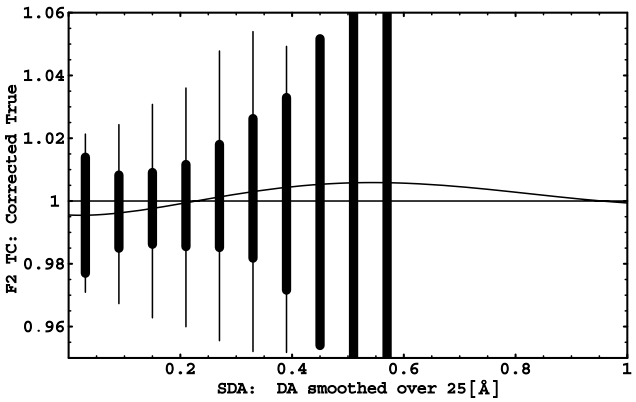

FIG. 4.—Fractional error in the partly corrected continuum level as a function of the mean amount of absorption. The points show the ratio of the continuum corrected for the SNR2 correlation to the true continuum in the artificial QSO spectra, F2/TC, as a function of the SDA. The thick bars indicate the mean and the error on the mean at each SDA value. The thin bars show $\pm 1\ \sigma$ for the F2/TC evaluated in all pixels in the SDA interval. The smooth curve is the function we used to implement the SDA correction.

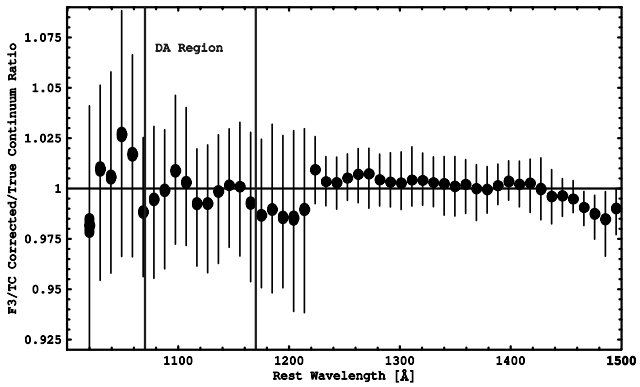

FIG. 5.—Fractional error in the fully corrected continuum level as a function of rest wavelength. We show the ratio of our F3 continuum to the true continuum in our sample of artificial spectra. The F3 continuum has our SNR2 and SDA corrections applied for $\lambda_r < 1216$ Å, while for higher wavelengths the F3 continuum is the original F1 continuum. The two vertical lines show 1070 and 1170 Å, the boundaries of the region where we measure the DA.

the total DA was 0.1583, which is 0.1% less than the DA = 0.1585 for this wavelength range in the input artificial spectra.

The effect is similar for the Kast spectra: We had DA = 0.1637 using the F1 continua, and we find DA = 0.1533 using the F2 continua. DA(F1) was too large by 6.8%, similar to the excess for the artificial spectra, but not identical because the distribution of flux as a function of SNR2 is different.

5.2. *Correcting the Continua of the Artificial Spectra Using SDA*

We define a second variable, which also indicates regions of the spectra where we might have made systematic errors in the continuum fits. The SDA is the smoothed DA, obtained by smoothing the flux with an exponential filter with FWHM 25 Å rest. This length is similar to the scales on which we see strong correlations in the continuum errors.

In Figure 4 we show the F2/TC as a function of the SDA. We see a systematic trend that indicates that F2 is too high by about 1% on average in regions of the artificial spectra that have $0.3 < \mathrm{SDA} < 0.6$. We used the smooth curve to approximate the corrections that we made to F2 to remove this trend. We show how we extrapolated the curve to higher SDA values that occur in some parts of the Kast spectra, but not in the artificial spectra, because the artificial spectra differ from the Kast spectra.

We label F3 the continua that we corrected for the SDA correlation (F2 to F3) after we had corrected them for the SNR2 correlation (F1 to F2). For the artificial spectra, the mean DA following the correction to F2 was 0.1585, and after the correction using the SDA the F3 continua gave DA = 0.1602. The change is 1.1%, which leaves the DA nearly identical to the known value, 0.1601, as required by the definition of the corrections.

For the Kast spectra, the change is a 1.2% increase, from DA(F2) = 0.1533 to DA(F3) = 0.1552. This is slightly different from the change to the artificial spectra because the distribution of the flux as a function of the SDA can differ from that for the artificial spectra.

In Figure 5 we see that F3/TC is a well-behaved function of rest wavelength. The thick bars show the mean values, from all QSOs (usually 77) that contribute at that wavelength. The mean F3/TC across the DA region is near 1.0 by definition of the corrections. About 16% of pixels have F3/TC < 0.96 and 16% are greater than 1.03, with little variation across the DA region. We are not surprised that the mean F3/TC values are correlated over many pixels and regions of around 60 Å because the continuum errors F1/TC were also correlated over such large scales. We also see a tendency for the F3/TC to be too low in the interval 1170–1216 Å. We saw that we fitted the continuum too low in this region for some QSOs.

In Figure 6 we show the standard deviation of the F3/TC values, σ(F3/TC), as a function of λ_r. The value is nearly constant, around 1.3% at greater than 1220 Å. It peaks near the peak of Lyα, at 4.5%, declining slowly as we move down the blue wing of Lyα. It rises again below 1070 Å, reaching a level of 5%–6%. We used this figure to help us choose the DA region.

5.3. *Effects that May Remain Uncorrected*

Here we discuss two of several possible sources of error in our continuum estimates that the SNR2 and SDA corrections may have missed.

First, there are errors in the flux values in our QSO spectra due to the limitations of the flux calibration procedure applied to the observed spectra. There are numerous sources for such errors, which we describe in detail in (Suzuki et al. 2003). Fortunately, many flux calibration errors in low-resolution spectra vary smoothly over large scales greater than 50 Å, and they will

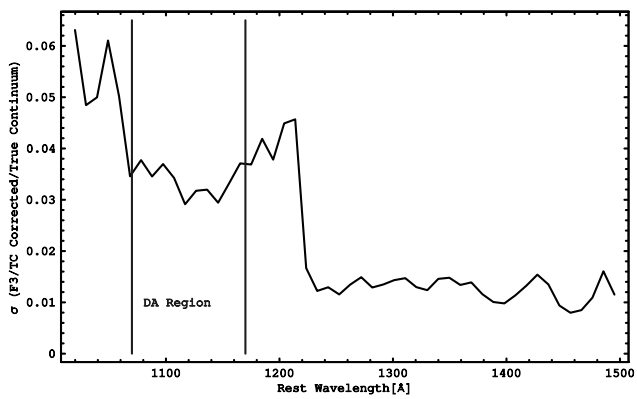

FIG. 6.—Standard deviation of the fractional error in our continuum fits to the artificial spectra, F3/TC. Our continuum fits appear to be well behaved in the region we use to measure the DA: $1070 < \lambda_r < 1170$ Å.

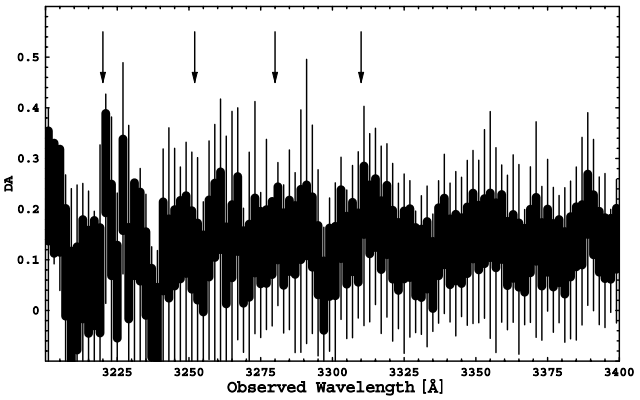

FIG. 7.—Total amount of absorption, shown as DA, in the Kast spectra as a function of observed wavelength where ozone absorption is expected. We expect the most ozone absorption and the highest DA values near the marked wavelengths, 3198, 3220, 3252, 3280, and 3310 Å. As in previous figures, the center of each thick bar is at the mean DA value in the bin, and its length is the $\pm 1\ \sigma$ error on the mean, while the thin lines extend to $\pm 1\ \sigma$ for the DA values per pixel.

mostly have been absorbed as adjustments to the continuum fit, reducing their effect on the DA. Some of these errors might vary randomly in sign from QSO to QSO, and with wavelength, leading to a minimal net effect in our sample, but others are systematic.

An example of a systematic flux error is the strong atmospheric ozone absorption that varies in strength with a period of about 25 Å and increases greatly below about 3310 Å (Schachter 1991). We did not explicitly remove the ozone absorption from either the standard stars or the QSO spectra; hence we expect to see this pattern in the Lyα forest absorption. In Figure 7 we show the DA as a function of observed wavelength. Some variations can be seen at rest wavelengths of less than 3250 Å, which are probably due to ozone absorption. However, we note that the variations go both high and low, because we generally fitted continua through ozone absorption, not above or below it, so the net effect on our estimated DA should be minimal.

Second, it is possible that the artificial spectra differ from the Kast spectra in some way that is difficult to notice but nonetheless very important. We discuss two examples: strong and weak Lyα lines.

We know that the artificial spectra lack strong Lyα lines from high-density regions that have high $N_{\rm H\,I}$. As we show in § 7, in the Kast spectra these lines are expected to have DA = 1%. In § 5.2 we found that we did not make unusual continuum fits in regions with the most absorption. This is because we place continuum control points approximately every 50 Å, and we tried hard to keep the continuum smooth on much larger scales in the DA region. The Kast spectra are well suited to giving smooth continua because they are of low resolution with good relative flux. The Lyα lines of systems with large $N_{\rm H\,I}$ have little effect on the continuum fits. The Lyα line of LLSs that are not DLAs have equivalent widths that are insignificant compared to the 25 Å of the spectrum, and the DLAs are too rare, only about six in the Kast spectra, to have a major effect on the continuum errors.

What if the Kast spectra also have some smoothly varying absorption that covers many wavelengths but is not included in the simulations? Since we examined the whole of each spectrum, from near C IV to below Lyβ, we hope that we have correctly accounted for such hypothetical absorption. However, the F3/TC will not tell us if we erred.

In summary, we are reasonably confident that we have accounted for the main systematic effects.

6. DA IN KAST SPECTRA

We applied exactly the same corrections to the Lyα forest of the Kast continua as we applied to the artificial ones to make the equivalent of F3 for the Kast spectra. We will no longer mention the uncorrected continua on the Kast spectra. Hence, the DA in a pixel, which we label DA0, is the flux divided by the corrected continuum fit, F3. For the Kast spectra, we can not show ratios such as F3/TC, since we do not know the true continuum level.

In Figure 8 we show two statistics from the DA0 values. The thin vertical lines show the $\pm 1\ \sigma$ of the DA0 values. The center of the short solid bars show the mean DA0 from all DA0 values in the 4.5 Å rest-frame wavelength regions, which we call DA1. The length of the thick bars show the $\pm 1\ \sigma$ errors on those means, calculated from bootstrap resampling the flux in the approximately 900 pixels in each wavelength bin. We also show the DA wavelength range. We make several points from this plot that guide our decisions on how we measure the overall mean DA4 value.

First, at 1225–1500 Å there is clearly absorption due to metal lines. The mean is around 2%, systematically increasing to smaller wavelengths. We discuss this below.

Second, the DA1 values rises smoothly as we cross the peak of the Lyα line. The transition across the Lyα emission lines is wide, from about 1210–1225 Å, a range of around 3700 km s^{-1}. We see that the DA1 near the wavelength of the peak of Lyα (the lower end of the arrow labeled Lyα emission) is near the mean of the DA1 on either side of Lyα. This trend comes from the proximity effect, modified by the errors in the $z_{\rm em}$ values that we used and the large errors in continua near the peaks of the emission line. We would need to improve these two factors before we could use these data to measure the proximity effect.

Third, the DA1 is approximately constant across the DA region.

Fourth, the DA1 is higher in 1190–1205 Å. This might be related to the continuum fitting errors that made the F3/TC too low for 1170–1220 Å for the artificial spectra (Fig. 5).

Fifth, the DA1 is higher at 1000–1045 Å. Some of this might be from continuum errors that increase as the S/N decreases. Figure 5 showed that the F3/TC values had a large σ at these wavelengths, and four of the five mean F3/TC values were

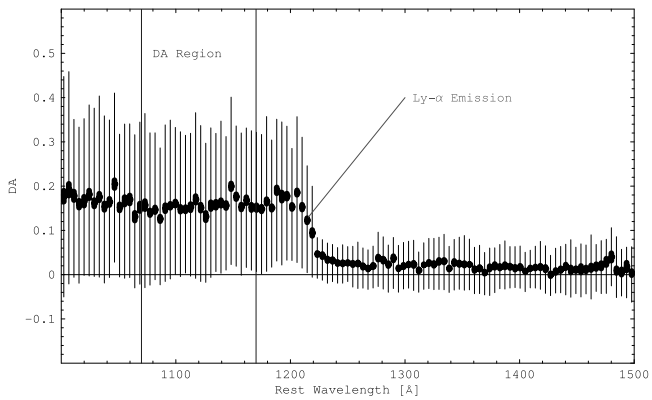

FIG. 8.—Total absorption in the Kast spectra, shown as DA, as a function of rest wavelength. The DA includes absorption by Lyα in the IGM, LLS, DLAs, and metal lines. The thin lines show the $\pm 1\ \sigma$ values for the DA0 per pixel. The heavy lines show the mean and error on the mean DA in the 4.5 Å bins, the DA1 values.

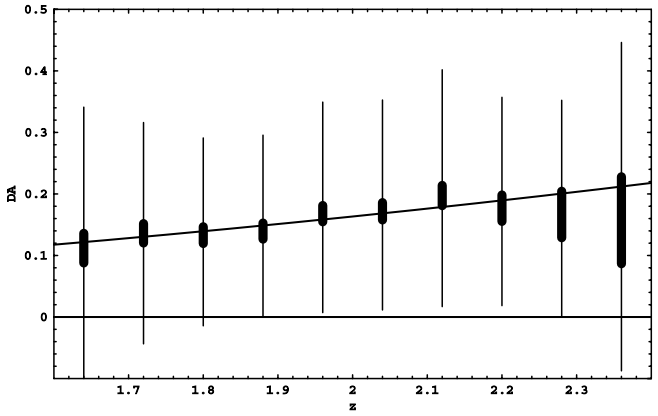

FIG. 9.—Total amount of absorption in the Kast spectra from rest wavelengths 1070–1170 Å as a function of Lyα redshift. We show the mean DA values for all pixels with z_{abs} in the indicated ranges. The measurements from each QSO contribute to 1–3 bins. The DA values include contributions from the Lyα in the IGM, in LLS, DLA*s*, and metal lines. The errors are as in similar figures.

slightly too high. Rather, the DA1 is probably higher because of absorption by Lyβ and perhaps some O VI.

Finally, there is some extra remaining dispersion in the DA1 in the Lyα forest because we have not yet removed the tendency for DA to increase with z.

6.1. *How DA Changes with z*

In Figure 9 we show the DA as a function of the Lyα absorption redshift. We give the values in Table 2. The thin lines are again the ± 1 σ of all the DA0 (pixel) values in each z bin, while the thick bars show the mean DA values, μ(DA) and their errors $\sigma(\mu)$, which we have underestimated. In Table 2 we also list the usual 1 σ confidence interval for the DA values per pixel. We give the critical DA values, where 15.8% of the values are below the lower value (col. [4]) and 15.8% are above the larger value (col. [5]). We see a slight increase in the DA with increasing z, as expected from well known counts of the number of lines per unit redshift, a trend first found by Peterson (1978). We fit this trend with

$$\mathrm{DA}(z) = A[(1+z)/(1+1.9)]^{\gamma}, \tag{5}$$

with $A = 0.147$ and $\gamma = 2.57$. These values are slightly different from those for the input artificial spectra: $A = 0.150$ and $\gamma = 2.07$. We do not quote errors on these parameters because the range of z covered is very small and the slope γ is not well determined. We concentrate instead on estimating the DA at the mean z for the sample.

7. Lyα ABSORPTION FROM HIGH COLUMN DENSITY LINES

Some of the absorption in the DA region is from the Lyα lines of systems with high H I column densities, the LLSs and DLAs. We now estimate how much, because these absorbers are much harder to include accurately in the numerical simulations that have the large boxes needed for the IGM. We expect that this is a temporary situation, since we would prefer to use simulations that include all the main features of the IGM and galaxies that are responsible for the absorption in QSO spectra. They should include realistic LLSs and DLAs, with realistic velocity structure, temperatures, and metal abundances, giving realistic metal lines.

We introduce

$$\mathrm{DA5}(z) = N(z) W_r (1+z)/\lambda_r \tag{6}$$

to estimate the amount of absorption from lines with a rest-frame wavelength λ_r, a density of $N(z)$ lines per unit z and a mean rest-frame equivalent width W_r (Å). The $(1+z)$ factor converts W_r to the observed frame. A unit of z for Lyα corresponds to an observed wavelength interval of 1215.67 Å.

LLSs with $\log N_{\mathrm{H\,I}} > 17.2$ cm^{-2} have Lyman continuum optical depth of less than 1 (Tytler 1982) and a density $N(1.9) = 1.4 \pm 0.5$ (from Fig. 2 of Stengler-Larrea et al. 1995). The fractional error is huge because *HST* has obtained spectra of few QSOs that could show Lyman limits around 2650 Å. We measure a mean $W_r = 3.0 \pm 0.5$ Å for 66 LLSs and DLAs measured in Kast spectra, and calibrated with 13 systems that we also observed with HIRES (Burles 1997). These LLSs and DLAs were detected as Lyman limits at $2.4 < z < 4.1$. We ignore possible evolution in this mean W_r. We obtained the error by summing three terms in quadrature: 0.2 Å from the calibration, 0.3 Å from the sample size, and 0.3 Å for possible bias in the sample. The W_r values have an approximately exponential distribution for small W_r values, with an excess at the largest values from DLAs (Sargent et al. 1980).

Using the values above, we find the contribution to the DA from Lyα lines at $z = 1.9$ in systems with $\log N_{\mathrm{H\,I}} > 17.2$ cm^{-2} is

$$\mathrm{DA6}s = 1.0 \pm 0.4\%, \tag{7}$$

where nearly all of the error is from the uncertain number of LLSs at $z = 1.9$. Here and elsewhere, the suffix "*s*" refers

TABLE 2
TOTAL ABSORPTION DA AS A FUNCTION OF REDSHIFT

z	Mean DA	$\sigma(\mu)$	15.8% Below	15.8% Above
1.64	0.1107	0.0241	−0.133	0.341
1.72	0.1341	0.0157	−0.047	0.315
1.80	0.1308	0.0136	−0.018	0.289
1.88	0.1375	0.0130	−0.002	0.294
1.96	0.1662	0.0132	0.004	0.349
2.04	0.1702	0.0141	0.009	0.353
2.12	0.1961	0.0165	0.014	0.402
2.20	0.1754	0.0215	0.016	0.359
2.28	0.1653	0.0378	−0.001	0.352
2.36	0.1556	0.0706	−0.090	0.447

to a value for $z = 1.900$. Too few LLSs are known at redshifts 1.5–2.5 to determine how the number per unit redshift changes with redshift.

We checked this result using only the DLAs with $\log N_{\rm H\,I} > 20.2$ cm^{-2}, or $W_r > 10.3$ Å. The DLAs have $N(z = 1.9) = 0.20 \pm 0.04$ from Storrie-Lombardi & Wolfe (2000, Fig. 11), and their mean $W_r = 17.78$ Å, from their equation (3) and Wolfe et al. (1986, eq. [3]). This mean is for DLAs observed at $1.5 < z < 4$. They have DA = 0.85% ± 0.17%, where we have ignored the large and poorly known error on the mean W_r (MW04, end of Appendix B). We expect this DA to be smaller than that for all LLSs, but the difference is less than we expected. Perhaps the DA6*s* value is too small. The LLSs and DLAs have independent normalization, each has a large statistical error, and we have ignored evolution of the W_r values.

8. ABSORPTION FROM METAL LINES

To measure absorption by metal lines alone we now introduce

$$\mathrm{DM} = 1 - \langle F \rangle, \quad (8)$$

where $F = 1$ if there is no metal line absorption. Since we defined DA to included all types of absorption, DM ≤ DA in the DA region. We measured DM in the λ_r range 1225–1500 Å, and we extrapolated to estimate a value for DM in the DA range 1070–1170 Å.

In Figure 10 we show the DM as a function of rest wavelength. We measure DM using the original continuum fits to the Kast spectra, without the corrections for correlations with SNR2 and SDA that we determined for the Lyα forest. Before making this plot we have measured the DM at the same wavelengths in the artificial spectra. Except for continuum level errors, this should be identically zero, since there are no metal lines in the artificial spectra. We saw slight absorption at all wavelengths, showing that we typically place the continuum too high by 0.5% (about 0.15 σ pixel^{-1}), and we subtracted this from the Kast spectra to give the DM that we show. A straight line fit to these DM values from $1225 < \lambda_r < 1500$ Å gave

$$\mathrm{DM1}(\lambda_r) = 1.585 - 2.67135 \times 10^{-4}(\lambda_r - 1360)\%, \quad (9)$$

where the λ_r value is in Å, and DM1 increase slightly as λ_r drops. However, a fit as a function of observed wavelength, λ_o (Å) gives

$$\mathrm{DM2}(\lambda_o) = 1.576 + 9.661 \times 10^{-4}(\lambda_o - 4158)\%, \quad (10)$$

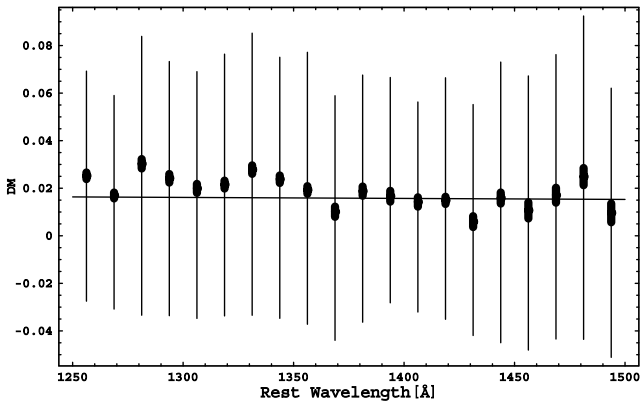

FIG. 10.—Amount of absorption in the Kast spectra from metal lines, DM, as a function of rest wavelengths. For our convenience, in this plot, we use DM values that we calculated using the raw fitted continua, without correction for the correlations with the SDA or SNR2. Because of this, the points are too high by an average of 0.495% and the mean value on the plot is 2.36%, instead of the correct value of 1.87%. Values can be negative because of photon noise and continuum fitting errors. The line is the DM1 fit.

which has a very similar mean near the mean wavelength, but now DM2 decreases as λ_o decreases. For the Kast spectra in the range 1225–1500 Å the mean $\lambda_o = 4158$ Å. We list this and other measurements of the metal absorption in Table 3.

We expect the DM1(λ_r) and DM2(λ_o) values to increase with decreasing λ for two reasons: additional lines are included at smaller λ_r, and the density of C IV lines increases at smaller redshifts, or observed wavelengths λ_o. However, the difference in the slopes of DM1 and DM2 indicate that the trend is not strong. Plots of these trends are not too helpful because they are dominated by the huge dispersion in the DM values, which makes it harder to measure the slope of DM with wavelength.

We define DM3(λ) as the mean DM in a segment of the spectrum of a QSO that is 121.567 Å wide in the observed frame, corresponding to $\Delta z = 0.1$ for Lyα. The DM3 values illustrate the huge dispersion in the DM across large parts of a spectrum. We began the first segment for a QSO at 1225 Å in the rest frame, the next one started where the first one ended, and the last one ended before the minimum of the maximum observed wavelength and 1500 Å. We ignored the remaining part of each spectrum that gave incomplete segments covering less than 121.567 Å near the maximum wavelength.

In Figure 11 we show the DM3 values from the Kast spectra as a function of observed wavelength, expressed as redshift for

TABLE 3
ABSORPTION BY METAL LINES

Parameter	λ_r (Å)	$\lambda_{\rm obs}$ (Å)	σ (%)	Mean (%)	σ(Mean) (%)
DM1	1362	...	...	1.58	0.13
DM2	...	4158	...	1.58	0.13
DM3	1360	4135	2.5	1.87	0.13
DM4 SBS88	1358	4125	2.7	1.67	0.22
DM5 SBS88	1360	...	...	1.66	0.22
DM6 SBS88	...	4158	...	1.65	0.22
DM7(C IV)	...	4580	...	0.69	0.15
DM7(C IV)	1360	...	...	0.71	...
DM7(C IV)	1120	...	...	0.80	...
DM1-6	1120	...	...	1.92	0.42
DM*s*	1120	...	...	2.3	0.5

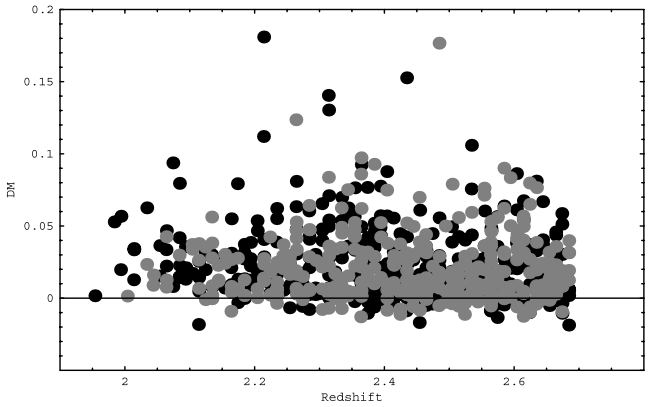

FIG. 11.—Amount of absorption by metal lines with $\lambda_r > 1215$ Å in the Kast spectra, DM2 values, as a function of redshift z for Lyα. Observed wavelength is $1215.67(1+z)$. The 377×2 DM2 values are the mean values, in adjacent segments of spectrum 121.567 Å long. The light points are from bins shifted from the dark ones by $\Delta z = 0.05$, one half the bin size of both points, hence most portions of a given spectrum contribute to two points. For our convenience, in this plot, we use DM2 values that we calculated using the raw fitted continua, without correction for the correlations with the SDA or SNR2. Because of this, the points are too high by an average of 0.495% and the mean value on the plot is 2.36%, instead of the correct value of 1.87%. Values can be negative because of photon noise and continuum fitting errors.

Lyα, to aid comparison with Figure 9. The mean of the DM3 values is $1.87\% \pm 0.13\%$, and the $\sigma(\mathrm{DM3}) = 2.5\%$ excluding photon noise, or 2.6% with the photon noise. The distribution of DM3 values is decidedly skew, with a long tail to huge DM3 values. Correlations amongst the DM3 extend right across a spectrum, because absorption systems with high $N_{\mathrm{H\,I}}$ values have many lines, these lines are strong, and they occur all over one spectrum. Moreover, systems are strongly clustered on scales up to 600 km s^{-1} (Sargent et al. 1988, hereafter SBS88).

8.1. *Measurement of DM Using Line Lists in Published Spectra*

We have measured DM4 values using the lists of absorption lines published by SBS88 for 26 QSOs with $1.7 < z_{\mathrm{em}} < 2.3$, excluding Q1510+115, which is BAL. Eleven of these QSOs are also in our Kast sample. We defined

$$\mathrm{DM4}(\lambda) = \sum_{\lambda i}^{\lambda i + 121.567} W_{\mathrm{obs}}/121.567 \text{ Å}, \qquad (11)$$

as an estimator of mean DM from all metal lines in bins of length 121.567 Å in the observed frame. As with the DM3 from the Kast spectra, the first bin started at the maximum of the minimum observed wavelength (SBS88, Table 1) and 1225 Å in the rest frame, and the last bin ended prior to the minimum of the maximum observed wavelength and 1500 Å. Each QSO contributed 4–7 segments, and we ignored the partial segments. The mean wavelengths were $\lambda_o = 4125$ Å and $\lambda_r = 1358$ Å. We took the observed frame equivalent width values W_{obs} from their Table 3. The results, in our Table 3, are similar to those from the Kast spectra: the mean of the 153 DM4 values was $1.67 \pm 0.22\%$ and the $\sigma(\mathrm{DM4}) = 2.74\%$. The mean is nearly identical to that for DM1 from Kast.

DM3 and DM4 differ in several ways. The most obvious difference between the distributions of DM3 and DM4 is that DM4 has a larger fraction of segments with DM $< 0.5\%$, those with few or no absorption lines. The DM3 values are effected by continuum errors, photon noise and weak absorption lines, all three of which are less prominent in the DM4 values. Typical weak lines in SBS88 have $W_{\mathrm{obs}} > 0.25$Å that individually give DM = 0.2%. Lines that are weaker than this will have been missed from DM4. The mean values are similar because weak lines do not produce a large part of the total absorption. Given this, the DM4 might have comparable accuracy to the DM3, since the smaller sample for the DM4 will be partly compensated by the lower sensitivity to continuum errors and photon noise.

We have fitted the DM4 values as a function of both λ_r and λ_o, giving

$$\mathrm{DM5}(\lambda_r) = 1.662 - 5.511 \times 10^{-3}(\lambda_r - 1360)\%, \qquad (12)$$

$$\mathrm{DM6}(\lambda_o) = 1.649 - 7.136 \times 10^{-5}(\lambda_o - 4158)\%. \qquad (13)$$

As with the DM1 and DM2 fits to the Kast metal lines, the mean values are similar and the slopes differ. This time the fit to the λ_r has the shallower slope.

8.2. *Absorption by* C IV

SBS88 and Steidel (1990) found that the number of C IV absorption lines increases as z decreases, and recent measurements show the same trend (Misawa et al. 2002).

We have estimated the DM due to C IV alone using equation (12) of SBS88. By definition, the total absorption from the stronger of the C IV doublet lines, 1548, is $N_* W_*$, per unit z. We obtained this by integrating the $n(W_*)$ equivalent width distribution over all W_r, from zero to infinity. This involves an extrapolation to $W_r < 0.15$ Å that is probably not much in error because the strong lines that were measured by SBS88 dominate the total absorption. Then

$$\begin{aligned}\mathrm{DM7}(1548, z = 1.957) &= N_* W_* (1+z)/1548 \\ &= 0.404\% \pm 0.074\%, \end{aligned} \qquad (14)$$

where the $(1+z)$ factor converts W_r to an observed equivalent width, and N_* is the number of lines per unit of z for this line, 1548 Å in the observed frame. We use $W_* = 0.46 \pm 0.04$ Å and $N_* = 4.60 \pm 0.74$ for their sample A4, and we assume that the sample is at about the redshift of their sample S2, 1.957. From their Figure 10, at this z the mean $W_r(1548)/W_r(1550) = 1.42 \pm 0.10$; hence,

$$\begin{aligned}\mathrm{DM7(C\ IV}, z = 1.957) &= \mathrm{DM}(1548) + \mathrm{DM}(1550) \\ &= 1.704 W_r(1548) = 0.69\% \pm 0.15\%. \end{aligned} \qquad (15)$$

The absorption due to C IV increases slightly as wavelength decreases. We make two simple assumptions to measure this trend. First, we scale the DM7(C IV) by a factor $[(1+z)/2.957]^{\gamma}$, whereas Misawa et al. (2002) find $\gamma = -0.58 \pm 0.46$ for their sample EM15, which includes 136 C IV systems with $W_r(1548) > 0.15$ Å. Second, we convert the z_{abs} for C IV(1548) to λ_r for Lyα by assuming that all our QSOs are at the mean $z_{\mathrm{em}} = 2.17$: $(1+z_{1548})1548 = \lambda_r(1+z_{\mathrm{em}})$. We find that DM(C IV) = 0.71% at $\lambda_r = 1360$ Å, which is 0.45 of the total DM1(1360).

8.3. *Extrapolating DM into the DA Region*

At the mean $\lambda_r = 1120$ Å, where we measure the DA, the four extrapolated DM values, DM1, DM2, DM5, and DM6, have a mean of

$$\mathrm{DM1} - 6(1120) = 1.92\% \pm 0.42\%, \qquad (16)$$

where the error is $\sigma/2$.

The DM increases in part because lines with smaller λ_r start to contribute in the spectrum at $\lambda < \lambda_r$. In the range $1225 < \lambda_r < 1500$ Å these include Si IV 1394, C II 1334, O I 1302, Si II 1260, and N V 1229. In the wavelength range 1070–1170 Å such lines include Si II 1193 and especially Si III 1206.

We increase our estimate of the DM in the Lyα forest by a factor of 1.2 ± 0.1 to account for the increasing number of lines as a function of decreasing λ_r because we suspect that these lines are not adequately accounted for by the trends with λ_r. The adjustment has a large error because it is based on our estimate of the fraction of the DM in the DA region that comes from metal lines not found at greater than 1250 Å. This estimate is highly uncertain because we have only nine spectra of high resolution at these redshifts. We will need a much larger sample for an accurate measurement.

The DM we use is then

$$\mathrm{DM}s(\lambda_r = 1120) = 2.3\% \pm 0.5\%, \qquad (17)$$

We estimated that had we been able to measure DMs values, in the Lyα forest, in bins of $\Delta z = 0.1$, those values would have $\sigma = 3.1\%$, which we obtain from $\sigma \propto$ (mean DM), using $\sigma(\mathrm{DM3}) = 2.5\%$ for mean DM3 $= 1.87\%$.

We find that the metals account for $15\% \pm 4\%$ of the total DA at $z = 1.9$. This is less than the estimate of Rauch et al. (1997), from a few QSOs, that about 22% of the total DA is from metals at $z \simeq 2$. If Rauch et al. (1997) used a path length of about $\Delta z = 0.9$ from about three QSOs, then their DM would have a relative error of order $3.1/(2.3\sqrt{9}) = 0.45\%$, sufficient that the difference from our estimate would not be significant. We also note that the Rauch et al. (1997) sample was biased to include sight lines with DLAs, which may also account for part of the difference.

9. DISPERSION OF DA VALUES

We have long known that there is a lot of scatter in the amount of Lyα forest absorption present in different low z_{em} QSOs (Carswell et al. 1982, § 7; Tytler 1987; Scott et al. 2000, Fig. 4; KCD01, Fig. 15; Kim et al. 2002, Fig. 8). Schaye et al. (2003) found that the χ^2 per degree of freedom of the DA measured in intervals of about $\Delta z = 0.2$ was 5.2 when they use all DA absorption, and it remained 2.4 after they had removed metal lines and DLAs. They stated that this residual scatter was probably cosmic variance.

We now measure the dispersion of the DA values measured in segments of spectra of length $\Delta z = 0.1$, and we estimate the individual contributions of the low-density IGM, the Lyα lines of the LLSs and the metal lines.

9.1. *DA2: The Mean DA in* $\Delta z = 0.1$ *Intervals*

We have already displayed the standard deviation of the pixel values of the DA, $\sigma(\mathrm{DA0})$, on various figures, and we saw that the values were large and similar in size to the mean DA values. A significant part of the $\sigma(\mathrm{DA0})$ values is from the photon noise. If there were no photon noise the $\sigma(\mathrm{DA0})$ values would be smaller than the standard deviation of the true flux from the QSOs, because the Kast spectra do not resolve the Lyα forest.

We define a DA2 value as the mean DA in a segment of the spectrum of one QSO that is 121.567 Å long in the observed frame, corresponding to 108 Kast pixels or $\Delta z = 0.1$. The velocity interval from one end of a segment to the other is 10335 km s^{-1} (Sargent et al. 1980, eq. [20]), and in a model with $H_0 = 71$ km s^{-1} Mpc^{-1}, $\Omega_\Lambda = 0.73$, and $\Omega_m = 0.27$, the interval $\Delta z = 0.1$ centered at $z = 1.9$ is 152.57 comoving Mpc.

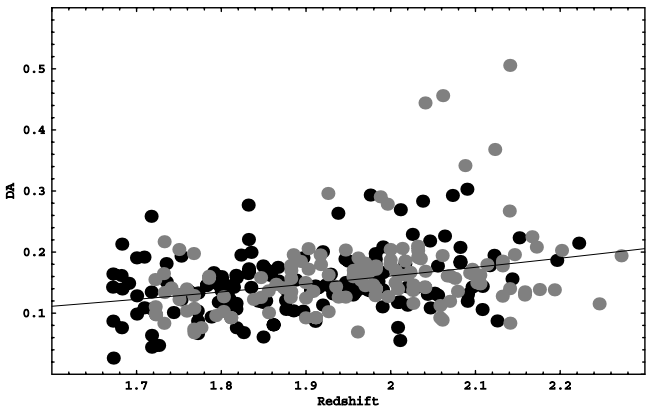

FIG. 12.—Total absorption in the Kast spectra in the rest-frame interval 1070–1170 Å as a function of redshift of Lyα. The absorption includes Lyα from the IGM, LLS, DLAs, and metal lines. The points are DA2 values, the mean DA in segments of length $\Delta z = 0.1$ or 121.567 Å in the observed frame. The solid line indicates the fit to the redshift evolution of the DA, given by eq. (5). The light points are from bins shifted from the dark ones by $\Delta z = 0.05$, one half the bin size of both points. Most of the largest values come from DLAs, some of which are split between two adjacent bins.

In Figure 12 we show the DA2 values from the Kast spectra. We started at the lowest z covered by each spectrum, and made points for each 0.1 segment, discarding the remainder of length less than 0.1 at the high-z end. This explains why there are many dark points at the lowest redshifts and few at the highest redshifts. We then added light points for bins starting at z values larger by 0.05, to better show the high redshifts and the DLAs. Many pixels contribute to both a dark and a light point on the plot. We also show the DA(z) curve from Figure 9.

To remove the portion of the dispersion in the DA that is due to the z trend, we define DA2s, where the suffix "s" refers to values scaled to the values we expect at $z = 1.900$ using the DA(z) trend from equation (5).

The contribution of photon noise to the standard deviation of the DA2s values, $\sigma(\mathrm{DA2}s)$, is small, except for a few segments. The $\sigma(\mathrm{DA2}s)$ from photon noise alone in a 108 pixel segment is 0.96% for S/N = 10 per pixel, rising to 3.8% by S/N = 5. The few segments with S/N < 5 are all in the lowest z_{abs} bin in Figure 12, and they alone have $\sigma(\mathrm{DA2}s) = 0.08$, while the remaining segments have the $\sigma(\mathrm{DA2}s) = 0.06$. The same applies to the equivalent point on Figure 9.

Figure 12 shows that the distribution is asymmetric, with a small fraction of segments having unusually large DA2 values. The three highest light points, all near $z = 2.1$ are due to DLAs. These DLAs do not show in the dark points because they are each accidentally split between two bins. The dispersion of the dark points about the mean DA (not the curve) is 6.81%, about half of the mean DA due to Lyα alone.

9.2. *Comparison of DA2s in Kast and Artificial Spectra*

In Figures 13 and 14 we show the distribution of DA2s in the Kast and the artificial spectra. We list parameters of the distributions in rows 1 and 7 of Table 4. We have not adjusted the artificial spectra to exactly match the absorption in Kast spectra, especially at this low z, and hence any agreement is accidental. We see that the two have similar mean DA2s; however, the Kast have a larger dispersion, as we might expect because they contain Lyα lines from the LLS and metal lines. In the second

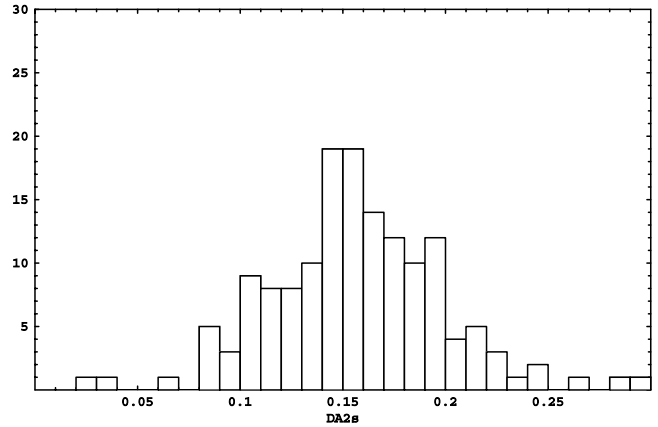

FIG. 13.—Distribution of DA2s values from the Kast spectra. The vertical axis shows the number of DA2s values. Each DA2s value is the mean DA in a bin of length $\Delta z = 0.1$. These DA2s values include absorption by metal lines and the Lyα lines from the IGM, LLSs, and DLAs. The values have been scaled, pixel by pixel, to the DA expected at $z = 1.9$ using the trend of eq. (5). Each portion of a spectrum contributes to a maximum of one value to this histogram. Unlike in Fig. 12, we do not use bins shifted by 0.05 in z. One DA2s value is too large to appear on the plot.

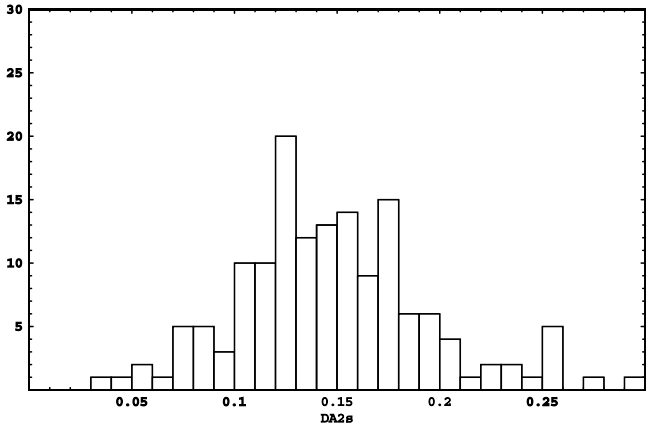

FIG. 14.—As Fig. 13, but for the artificial spectra from § 3 that we used to determine the corrections we applied to our continuum levels. All the DA2s values are shown.

row of Table 4 we also give statistics for just the segments with DA2$s < 0.35$. Both the mean and the standard deviation are reduced as we would expect, but the σ(DA2s) for the Kast segments remains larger by about 3 σ, than that for the artificial segments.

The approximate similarity of the artificial and Kast spectra means that the artificial spectra were well suited to help us find and remove the biases in the continuum fits. The artificial spectra accidentally contained about the correct total amount of absorption, although they were designed to model just the low-density IGM.

9.3. *Calculation of the Dispersion in the DA from the IGM*

We can calculate the expected variation in the amount of absorption in a spectrum. We restrict the calculation to the absorption from the Lyα lines in the lower density portions of the IGM, excluding absorption by the Lyα lines of LLSs and metal lines. We introduce the notation

$$\sigma(\Delta z) = \sigma(\text{DA2}s \text{ low-density IGM only}) \qquad (18)$$

for the standard deviation of the mean DA in spectral segments of length $\Delta z = 0.1$. The $\sigma(\Delta z = 0.1)$ values are the one-dimensional flux analog of the three-dimensional mass σ_8 values, (Kolb & Turner 1990, eq. [9.18] and Fig. 9.2). The $\sigma(\Delta z = 0.1)$ value is of great interest because it is a measure of the power in flux in the Lyα forest on scales of 153 Mpc, and it is related to the mass power spectrum.

McDonald (2003, Fig. 10a) shows that the relationship between the three-dimensional matter and flux power depends on scale. On large scales the flux power is proportional to the matter power, and hence to σ_8^2. On small scales an increase in the matter power leads to larger velocities that smooth the fluctuations in the flux and decrease the flux power. At a scale of $k \simeq 0.013$ (s km^{-1}) (1.5 Mpc) the flux power is insensitive to the mass power.

We can derive the variance of the DA2s values by integrating the power spectrum of the flux over a top-hat window function of width $\Delta z = 0.1$.

First we generate the one-dimensional flux power spectrum, $P_{F1D}(k)$, following McDonald (2003), Table 1. We use $\Omega_m = 0.23$, $\Omega_\Lambda = 0.73$, $H_0 = 71$ km s^{-1} Mpc^{-1}, $\sigma_8 = 0.9$, and $n = 0.95$. For these values, and $z = 1.9$, we calculate $\delta A_1 = 0.6375$, where A_1 is the amplitude of the mass power spectrum at wavenumber $k_1 = 2\pi(h^{-1}\ \text{Mpc})^{-1}$. We also use $\delta\overline{F} = 0.082$ to match the mean flux to our measured value, where $\overline{F} = 1-\text{DA}$ is the mean flux, and the δ values are the deviations from the values chosen by McDonald (2003). Then we calculate

$$\sigma(\Delta z = 0.1)^2 = \frac{\langle F\rangle^2}{2\pi}\int_{-\inf}^{\inf} P_{F1D}(k)W^2(k)dk, \qquad (19)$$

where $W(kR)$ is the top hat window function. We correct the result to our definitions of flux, since in our units McDonald (2003) uses $(F-)/\langle F\rangle$, a flux deviation divided by the global mean flux at that z. For the one dimensional case, we have

$$W^2(kR) = \frac{2[1-\cos(kR)]}{(kR)^2}, \qquad (20)$$

where $R = 152.57$ Mpc for $\Delta z = 0.1$.

We obtain $\sigma(\Delta z = 0.1) = 0.0386$ at $z = 1.9$ using $\sigma_8 = 0.9$, $n = 0.95$, and DA $= 0.118$ for the low-density IGM alone.

9.4. *Measurement of the Dispersion in the DA from the IGM*

A measurement of $\sigma(\Delta z = 0.1)$ has several uses. It provides a check on the linear model bias parameters $b_\delta'^2$ and β (McDonald 2003). The scale of $\sigma(\Delta z = 0.1)$ is large enough that we are well in the linear regime, and the astrophysical complications such as the detailed thermal history and temperature of the IGM and feedback will be less important than on small scales. If we know the bias parameters from calculations, we can calculate a normalization for the mass power spectrum that is a larger scale and earlier epoch analog of σ_8.

The $\sigma(\Delta z = 0.1)$ value is hard to measure because we must estimate and subtract the portion of the dispersion coming from the Lyα lines in LLSs, metal lines, and continuum fit errors.

In Table 4 we list the mean and σ of the DA2 values for the Lyα lines of LLSs (including DLAs). We calculate that σ(DA2) for the Lyα of LLSs is 0.035 by randomly sampling their W_r values. We have checked this result analytically. Since the expected number of LLSs per $\Delta z = 0.1$ is only 0.14, 0.869 of segments have none, 0.122 have one, and 0.009 have two or more, if we ignore clustering. We then obtain the approximate σ of the DA of the Lyα of the LLSs from the sum of the squares

TABLE 4
DISTRIBUTION OF THE DA2s AT $z = 1.9$ IN $\Delta z = 0.1$ SEGMENTS

Data Set	Metals?	LLS?	n	σ(DA2s)	$\sigma[\sigma$(DA2s)]	Mean DA2s	$\sigma\mu$
Kast spectra	Yes	Yes	152	0.0612	0.0035	0.1563	0.0050
Kast <0.35	Yes	Yes	151	0.0487	0.0028	0.1488	0.0049
Lyα of LLS	No	Yes	471:	0.0351	0.0047	0.0103	0.004
Metals (DM3, DMs)	Yes	No	377	0.031	...	0.023	0.005
$\sigma(\Delta z = 0.1)$ Kast IGM only	No	No	152	0.039	$^{+0.005}_{-0.007}$	0.118	0.010
$\sigma_{0.1}$ calculated	No	No	...	0.0386	...	0.118	...
Artificial spectra	No	No	150	0.0422	0.0024	0.1518	0.0035
Hydrodynamic spectra simulation A	No	No	150	0.0331	0.0019	0.1287	0.0027

of the W_r values. In Table 4 we also list the equivalent values for the metal lines alone, mean DM2 and its σ taken from the end of § 8.

Both the Lyα of LLSs and the metal lines have a much larger affect on the σ(DA2s) values than they do on the mean DA2s values. The standard deviations of the amount of absorption from the Lyα of LLSs, σ(DA2s), is about 3.4 times the mean value. Similarly, the metal line σ(DA2s) is 1.3 times the mean. Both distributions have long tails containing huge values. The two distributions are more asymmetric than either Poisson or exponential distributions, both of which have σ equal to their means.

We estimated the σ of the DA2s of the Lyα in the IGM alone, $\sigma(\Delta z = 0.1)$ by adding random contributions from the IGM, LLSs, and metals. We assume that the DA2s values for the Lyα forest alone are drawn from a normal distribution with mean 11.8% and the one free parameter, the unknown $\sigma(\Delta z = 0.1)$. We made mock DA2s values by adding together three random numbers:

1. DA2s from the Lyα forest alone—a random deviate from the normal distribution.
2. DA2s from the Lyα lines of LLSs—a randomly selected DA2s value drawn from the known distribution of W_r values for LLSs (including DLAs).
3. DM2s from the metals—a randomly selected DM2 value, scaled to 1120 Å.

The mean value of DA2s for these mock spectra does not change as we vary the $\sigma(\Delta z = 0.1)$ value. We found that the mean DA2s from the mock spectra was 0.151, about 1 σ lower than the mean DA2s that we give in Table 4, and identical within the errors to the value in Table 5, as expected, since we are using the same data. We estimate a 68% confidence interval of $0.032 < \sigma(\Delta z = 0.1) < 0.044$, with a best value of 0.039. For these values, the mock segments matched the observed σ(DA2s) $= 0.0612 \pm 0.0035$. Since we assume that the three random numbers are independent, the sum of their variances is equal to the observed variance (§ 11.1), and we obtain the mean $\sigma(\Delta z = 0.1)$ value directly, without the need for mock spectra.

The values we give for $\sigma(\Delta z = 0.1)$ may have a larger error than we have estimated, because the many factors that contribute to the measurement are not well known. The dispersions from the metals involves an extrapolation, and we have assumed that the contribution from the continuum error is insignificant.

The $\sigma(\Delta z = 0.1)$ value includes the dispersion from both the Lyα in the low-density IGM and the continuum errors, because we did not include the latter in a three part model for the mock segments. The dispersion of the DA in the artificial spectra, without noise or continua fits, was 0.0441. When we remeasured this dispersion after adding photon noise and fitting the continua we found 0.0422, from Table 4, which shows no significant increase from the fits. This implies that the continuum fits have an insignificant error. Below we will see that the dispersion from a hydrodynamic simulation suggests that our $\sigma(\Delta z = 0.1)$ value is approximately correct, and hence that the continuum error is not a major part of the value. However, if we treat the continuum fits as absorbed spectra, the dispersion of the equivalent DA is 0.0325, which suggests that the continuum error is a significant part of the $\sigma(\Delta z = 0.1)$ value. We intend to investigate this issue in future work starting with a fully automated continuum fitting algorithm that should be more stable.

The Lyα absorption from the low-density IGM, the Lyα from the LLS, and the metal lines all appear to contribute similar amounts to the dispersion in the DA2s values in $\Delta z = 0.1$ bins at $z = 1.9$. Kim et al. (2004, Fig. 3) showed that metal lines comprise a large part of the power on small scales ($k > 0.1$ s km^{-1}), but only 0.07 of the total power on scales $0.003 < k < 0.03$ s km^{-1}, or 200–2000 km s^{-1}. However, we must note that Kim et al. (2004) avoided sight lines with strong

TABLE 5
DA3s VALUES FOR QUARTERS OF THE SAMPLES OF KAST AND ARTIFICIAL SPECTRA

	ARTIFICIAL				
QUARTER (1)	True (2)	Measured (3)	True−Measured (4)	KAST MEASURED (5)	MEAN z_{abs} (6)
First	0.1574	0.1577	−0.00027	0.1487	1.949
Second	0.1668	0.1660	0.00075	0.1456	1.936
Third	0.1433	0.1486	−0.00531	0.1696	1.966
Fourth	0.1546	0.1449	0.00990	0.1404	1.846
σ	0.0097	0.0095	0.00634	0.0128	...
Mean μ	0.1555	0.1543	0.00127	0.1511	1.924
$\sigma(\mu)$	0.0048	0.0048	0.00317	0.0064	...

DLA absorption, so this may be an underestimate of the true metal line power. Since integrated power is proportional to variance, this implies that the metals will contribute about 7% of the variance on scales 200–2000 km s^{-1}. We find that the metals comprise $(0.031/0.0612)^2 = 0.26$ of the total variance sampled in bins with $\Delta z = 0.1$, or 10,335 km s^{-1}. On these large scales the dispersion due to the metals becomes a larger part of the total because the absorption by metal ions is strongly correlated across these large scales. A single absorption system can put strong metal lines all over a spectrum. The correlation arises from the multiplicity of strong spectral lines, and not from the distribution of matter on 153 Mpc scales.

Our $\sigma(\Delta z = 0.1)$ value may be too large because we ignored the correlation of LLSs and metal lines. The absorption systems that show many strong metal lines are likely to be LLSs. The DLAs in particular also have a lot of metal lines, especially when the gas covers a wide range of velocities, and the metal abundances are high. Hence the mock spectra that we made to calculate $\sigma(\Delta z = 0.1)$ would be more realistic if the we had chosen a large DM2 value, rather than a random one, whenever a segment had a Lyα with a large W_r value. This correction would make more segments with very large DA2*s* values, which would increase the variance from the metals and LLSs, and hence decrease our estimate of the $\sigma(\Delta z = 0.1)$. We have not modeled this complication, because the metal lines lie at specific velocities relative to the Lyα line and we should make complete mock spectra, with realistic mock absorption systems. Alternatively, and preferably, we could use spectra of high spectral resolution and remove the metal lines and the Lyα of the LLSs.

The $\sigma(\Delta z = 0.1)$ value that we measured, $0.039^{+0.005}_{-0.007}$ is identical within the errors to the value that we calculated: 0.0386 for $\sigma_8 = 0.9$ and $n = 0.95$. Systematic effects from the photon noise, continuum fit and LLS-metal correlations should all have made our measured value too large, and hence the errors in the measurement may be larger than the values we quote. For fixed n and a fixed and known (McDonald 2003) relationship between the flux and matter power spectra, $\sigma(\Delta z = 0.1) \propto \sigma_8$ and the errors that we quote on $\sigma(\Delta z = 0.1)$ imply $\sigma_8 = 0.90^{+0.13}_{-0.16}$. With improved measurements, quantities like $\sigma(\Delta z = 0.1)$ will provide useful new measurements of the matter power spectrum, on larger scales than have been explored using the flux power spectrum (Croft et al. 2002b).

10. DA3: THE DA IN QUARTERS OF THE SAMPLE

To obtain an accurate mean DA value we need to average over a substantial path length, from many lines of sight. If the DA0 values were independent deviates drawn from the same distribution (e.g. same S/N) we would expect that the standard deviations of the DA2*s* points would be about 10 times smaller than that of the DA per pixel, DA0, because there are about 108 pixels per DA2 point. However, $\sigma(\mathrm{DA2}s) = 6.12\%$, only 3 times less that $\sigma(\mathrm{DA0}s) = 20.3\%$.

We have explored the dispersion of the mean DA in much larger bins. We divided the spectra, both artificial and Kast, into four groups, or quarters, giving the DA3*s* values that we list in Table 5. We used equation (5) to scale these values to the expected value at $z = 1.9$, because the fourth quarter happened to have a significantly lower mean z. We assigned the QSOs to quarters in order of right ascension (R.A.), to emphasize a possible source of bias. QSOs with similar R.A. values are more likely to be observed at the same time, through similar conditions, giving more similar S/N, and to have their spectra reduced in the same way. Our initial continuum fits were also done in R.A. order, although later adjustments were done in order of emission line strength and S/N. The R.A. order of the artificial spectra is that of their partner QSOs.

The second column is the DA3*s* in the input artificial spectra, with flux range 0–1, plus photon noise. If the simulations were a faithful representation of the IGM absorption, the error on the mean of these values, $\sigma(\mu) = \sigma/2 = 0.48\%$ would be an estimate of the portion of the error in the DA from the 77 Kast spectra due to the sample size. From an examination of a much larger sample of similar artificial spectra, we calculate an expected $\sigma(\mu) = 0.4\%-0.5\%$ for a sample at $z = 1.9$ with a path length of 19.75.

This is the error we would have obtained had our spectra and the continuum fits been perfect. However, the artificial spectra have more absorption than the low-density IGM alone, and they lack high $N_{\mathrm{H\,I}}$ lines and metal lines. Hence the error for the Kast spectra will be somewhat larger.

Column (3) shows our measurements of DA3*s* values in the artificial spectra with emission lines and S/N like our Kast spectra. The dispersion in this column includes many effects, especially the continuum level errors and our corrections for the biases that we measured as a function of SNR2 and the SDA. The mean of this column is nearly identical to the equivalent values in column (2) because the corrections that we made to the continua forced agreement. The σ values are similar because the continuum fits did not increase the dispersion.

Column (4) shows the row by row difference between the DA3*s* values in the first two columns: the four true DA3*s* values, minus our measurement of each. The dispersion in this column is the portion of the measurement error coming from the S/N, and especially our continuum fitting and continuum level corrections. The error on the mean of $\sigma(\mu) = 0.32\%$ is again less than the error in the column (2), 0.48%. This implies that our spectra, their S/N, our continuum fits, and our corrections to the continuum fits are adequate for a sample of 77 QSOs at $z = 2$.

Column (5) shows the DA3*s* values for the quarters of the Kast QSO spectra. The error on the mean is the largest of the values for the different columns, as expected, because we are now sensitive to the large $N_{\mathrm{H\,I}}$ lines and metal lines. We already saw working with the DA2*s* $\Delta z = 0.1$ values that the metal lines and the Lyα of LLSs have a large effect.

11. ERRORS ON THE DA MEASUREMENTS

We first discuss how the error on the DA measurements decreases with as we increase the redshift path length, and then we give our best estimate for the DA and the associated error.

11.1. *How the Error on the DA Depends on Sample Size*

We find that the standard deviation of a measurement of the DA decreases with increasing sample size, but not as rapidly as expected for independent random samples from the same distribution function. We first concatenated the spectra of the DA regions in all the Kast spectra. The result is a list of fluxes in approximately 19,000 pixels, where each QSO contributes a continuous segment of approximately 250 pixels. We join the spectra in RA order, the same order we use for the DA3 values. We compute the mean DA values in segments containing different numbers N of adjacent pixels. Longer segments always contain flux values from more than one QSO, as do some short segments.

In Figure 15 we show the standard deviation of the mean DA values, as a function of N. The standard deviation of the

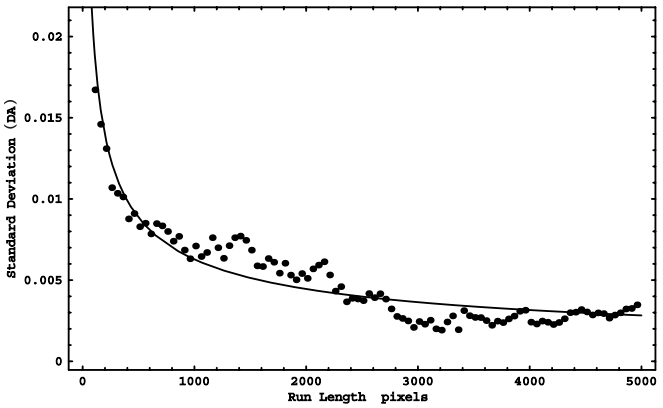

FIG. 15.—Estimate of our error in measuring the DA as a function of the number of pixels N in the DA region of the Lyα forest. The vertical axis shows the standard deviation of the mean DA values. The horizontal axis shows the number of adjacent pixels N used to calculate each mean DA value. We find that the standard deviation falls as $N^{-0.37}$, as indicated by the solid curve.

mean DA values follows $\sigma_N \propto N^{-0.37}$, over a large range of N. However, if we select the N pixels at random, then $\sigma_N \propto N^{-0.5}$.

If the DA values of the pixels are independent random variables, with means μ_i and variances σ_i^2, then a sum of the DA values has variance $\sum \sigma_i^2$, and the mean DA has standard deviation $\sigma_N = (\sum \sigma_i^2/N)^{0.5}$. We find $\sigma_N \propto N^{-0.37}$ because the DA values in adjacent pixels in an individual spectrum are correlated. The correlation is mostly from the structure of the IGM, and from continuum level errors, both of which correlate the DA values. There is also a small effect from the few spectra with low S/N values that give unusually large σ_i values.

We use the relationship in Figure 15 to estimate the errors on mean values of the DA when appropriate (Table 2, Figs. 4 and 9). We use bootstrap resampling error estimates otherwise (Figs. 5, 7, 8, and 10), including all plots that extend to $\lambda_r > 1215$ Å.

11.2. *Our DA Measurement and Its Error*

The absolute 1 σ error terms associated with our DA4 estimate are the following:

1. First, 0.64% estimated from the dispersion in quarters of our sample (Table 5, col. [6]). This includes sample variance and that part of the calibration error that varies between the quarters.
2. Calibration error of 0.32%, from Table 5, column (5). Estimate of the error in the corrections that we applied to the continuum levels that correlated with SNR2 and the SDA.
3. Sample variance of 0.48% from the size of our sample (sometimes called cosmic variance).
4. Uncertainty of 0.5% from the uncertainty in the amount of metal absorption.
5. Uncertainty of 0.4% from the uncertainty in the amount of absorption from Lyα lines with $\log N_{\rm H\,I} > 17.2$ cm^{-2}.

To obtain DA4s, we first scaled the DA0 values for each pixel to the expected value at $z = 1.9$, using equation (5), before taking the mean. The result is slightly different from a scaling of the mean DA4, using the single mean $z_{\rm abs}$ value. As our estimate of the error on our DA4s measurement we use the quadratic sum of the errors on the first two terms above, giving

$$\mathrm{DA4}s(z = 1.9) = 15.1\% \pm 0.7\%, \qquad (21)$$

where the suffix "s" means that the value applies to $z = 1.900$.

For comparison with measurements or simulations that do not include metal lines, we can subtract DM$s = 2.3\% \pm 0.5\%$ for the metal lines, giving DA7s = DA4s − DMs, or

$$\mathrm{DA7}s(z = 1.900) = 12.8\% \pm 0.9\%, \qquad (22)$$

and for comparison with data or simulations that include neither metal lines nor Lyα lines from systems with $\log N_{\rm H\,I} > 17.2$ cm^{-2} (all LLSs and DLAs) the appropriate DA is DA8s = DA4s − *DA*6s − DMs, or

$$\mathrm{DA8}s(z = 1.900) = 11.8\% \pm 1.0\%. \qquad (23)$$

When we subtract DA values we should first convert them to optical depth, subtract, and then convert back to DA. We did not do this because it further complicates the flow of values from the data to results and makes little difference for small DA values.

12. COMPARISON WITH HYDRODYNAMIC SIMULATIONS

In this section we compare the DA from the Kast spectra to values from full hydrodynamic numerical simulations. We give a more thorough description in T. Jena et al. (2004, in preparation).

We use the cosmological simulation code ENZO (Norman & Bryan 1999), which follows both dark matter dynamics and hydrodynamics consistently. The collisionless dark matter particles are evolved using a Lagrangian particle-mesh method, whereas the equations of gas dynamics are solved using a piecewise parabolic (PPM) method.

The simulations use the evolving UV background radiation field due to both QSO and stellar sources described by Madau et al. (1999). From this spectrum we calculate photoionization and photoheating rates for H I, He I, and He II.

We make the common assumption that the gas is optically thin, so that all particles experience the same photon flux. Although we believe that we have the appropriate level of ionization in the low-density IGM, the gas remains optically thin in the simulation even in high-density regions; hence we overionized the densest regions, the spectra do not include any LLSs or DLAs, and we underestimate the temperature at higher redshifts, until long after the gas has been ionized (Bolton et al. 2004). The simulation does not include star formation or any related feedback such as winds (Croft et al. 2002a).

We used a spatially flat ΛCDM universe with the parameters in Table 6. We used an initial power spectrum index $n = 1.00$, and we normalized the power spectrum to $\sigma_8 = 0.9$. The parameter values are similar to the best-fit values using the *Wilkinson Microwave Anisotropy Probe* (*WMAP*) first-year data (Spergel et al. 2003), but we chose a slightly larger σ_8 consistent with other measurements cited in Spergel et al. (2003, Tables 2 and 4). The initial perturbations were assumed to arise from a Harrison-Zel'dovich power spectrum with the CDM transfer function of Eisenstein & Hu (1999). These density perturbations were then converted to initial velocities using the Zel'dovich approximation.

We ran one large simulation, A, with a box size of 54.528 h^{-1} Mpc, or 76.8 comoving Mpc, with 1024^3 cells for the baryon fluid containing 1024^3 dark matter particles. This simulation has 75 kpc resolution and is large enough to included the effects of some of the larger scale power missing from smaller boxes. It helps us measure the variation in the DA on the largest scales. It

TABLE 6
HYDRODYNAMIC SIMULATIONS OF THE IGM

Simulation	A	B	C, D, E
Baryon density Ω_b	0.0440	0.0440	0.0440
Matter density Ω_m	0.27	0.27	0.27
Vacuum energy Ω_Λ	0.73	0.73	0.73
Hubble constant H_0 (km s^{-1})	71	71	71
Power spectrum amplitude σ_8 ($n = 1$)	0.9	0.9	0.94
H I ionization rate γ_{912}	1.0	1.0	1.2
Enhanced He II ionization rate γ_{228}	1.8	1.8	1.4, 3.4, 5.4
Number of cells and dark matter particles	1024^3	256^3	256^3
Comoving box size (h^{-1} Mpc)	54.528	6.816	13.632
Comoving box size (Mpc)	76.8	9.6	19.2
Comoving resolution (cell size, kpc)	75	37.5	75

ran on the Blue Horizon computer at the San Diego Supercomputing Center.

We checked that our box was large enough to give reliable DA values. The DA for 75 kpc resolution simulations with box sizes of 9.6, 19.2, and 38.4 Mpc is 0.111, 0.103, and 0.104 at $z = 2$. Thus a 19.2 Mpc box size is enough for convergence of DA to within 0.01.

We increased the He II photoheating rate by a factor γ_{228} from that implied by Madau et al. (1999) to match the widths of Lyα lines described by the b-value distribution. Bryan & Machacek (2000) have shown that $\gamma_{228} \simeq 2.4$ gives enough heating in a simulation with 37.5 kpc resolution to approximately match the b-value distribution of the Lyα forest at $z \simeq 2.7$. We describe below in § 12.2 why we use $\gamma_{228} = 1.8$ for the 1024^3 simulation A. The enhanced γ_{228} corrects for heating that we miss because all our simulations are optically thin (Abel & Haehnelt 1999). It does not imply that the UVB has enhanced flux at $\lambda < 228$ Å.

We experimented with a smaller 9.6 Mpc box size to check that we had adequate resolution. We ran simulations in 64^3, 128^3, and 256^3 cubes. They have resolutions of 150, 75, and 37.5 kpc respectively, and they give DA values of 0.33, 0.32, and 0.32 at $z = 3$. Thus a resolution of 75 kpc gives convergence to within 1% for the DA. However, we use 37.5 kpc resolution simulation B in § 12.2 when we need convergence for absorption line b-values. Bryan & Machacek (2000) found that a 9.6 Mpc box with 37.5 kpc resolution gave adequate resolution for the b-values.

We make three points about the comparison of the hydrodynamic simulation and the Kast spectra.

First, we should compare the simulated spectra to the DA values for the IGM only, without metal line or the Lyα of LLSs.

Second, we made 150 simulated spectrum segments by passing lines of sight through the 76.8 Mpc volume. The error on the DA was $\simeq$0.6% for only 50 spectra, so 150 will give adequate accuracy. To obtain one segment, the line of sight traveled about 2 times through the box. The dispersion of the simulated spectra is reduced because the same modes, both the short and especially the long ones, are sampled many times.

Third, the simulation was made in a 76.8 Mpc box that contained no power on scales $\geq$38.4 Mpc and reduced power on somewhat smaller scales because the boundary conditions were periodic.

We list the results from the spectral segments of length $\Delta z = 0.1$ from the 1024^3 hydrodynamic simulation A in the eighth row of Table 4, along with the other comparable measures of the DA2s. In Figure 16 we show the distribution of DA2s from the hydrodynamic simulation A. The mean DA2s = 12.87% ± 0.27% is 1.08 ± 0.09 times that for the Kast IGM only from Table 4. The simulation A had slightly too much absorption. The σ(DA2s) of the simulated spectra was 0.85 ± 0.14 times the $\sigma(\Delta z = 0.1)$ from the Kast IGM only, slightly too small. We expect the simulations to have the same mean and a smaller σ than the Kast IGM-only values.

If we change the parameters in simulation A to reduce the mean DA, the σ(DA2s) will also decrease, and it is already smaller than the Kast IGM value. However, we expect the simulation σ(DA2s) to be smaller than the Kast, because of the finite size of the simulation box, and it is beyond the scope of this paper to determine whether the reduced value would be compatible with the spectra. However, in T. Jena et al. (2004, in preparation) we show that the power of the flux in spectra from simulation A does approximately match that in HIRES spectra on much smaller scales, $0.008 < \log k < 0.08$ (s km^{-1}) at these redshifts.

12.1. *How DA Depends on the Parameters of the Simulation*

There are at least six parameters of the simulation that we can adjust to better match the DA of the Kast spectra. We introduce γ_{912} for the rate of photoionization of H I in units of the rate predicted by Madau et al. (1999). First, we discuss γ_{912} and σ_8 together. Then we discuss $\Omega_b h^2$, Ω_Λ, the Hubble constant, and lastly in § 12.2, γ_{228}.

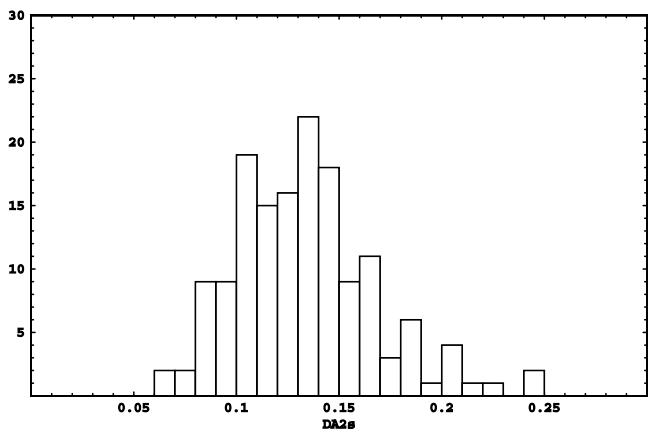

FIG. 16.—As Fig. 13, but showing DA2 values for spectra from the full hydrodynamic simulation A of the IGM, in a 75.7 Mpc box with a grid size of 1024^3. The simulation does not include Lyα from the LLS and DLAs, and it does not include metal absorption, unlike the data in Fig. 13. The bins were taken between $1.9 < z < 2.0$, and the simulation evolved slightly in this interval. We did not scale these DA2 values to $z = 1.9$.

TABLE 7
COSMOLOGICAL PARAMETERS DERIVED FROM OUR MEASUREMENT OF DA AT $z = 1.9$

Parameter (1)	Nominal Prior (2)	Derived from DA (3)	σ(derived)/derived (%) (4)	δ DA from σ(prior) (5)
Baryon density Ω_b	0.0444 ± 0.0018	0.0417 ± 0.0022	5	+0.008
Vacuum energy density Ω_Λ	0.73 ± 0.03	0.69 ± 0.04	6	+0.008
Hubble constant H_0 (km s^{-1} Mpc^{-1})	71^{+4}_{-3}	78^{+8}_{-7}	10	−0.005
Power spectrum amplitude σ_8 ($n = 1$)	0.9 ± 0.1	0.94 ± 0.04	4	−0.025
H I ionization rate γ_{912}	1.0 ± 0.1	1.08 ± 0.08	7	−0.012
Enhanced He II ionization rate γ_{228}	1.8 ± 0.6	3.2 ± 1.4	44	−0.006

In Table 7 we list nominal prior values for these six parameters from the following sources: Ω_b, h, and σ_8 from Spergel et al. (2003), γ_{912} from Madau et al. (1999), and γ_{228} from § 12.2.1. We use these values and errors to illustrate the sensitivity of the DA to the different parameters. We do not imply that they are the best-known values.

In column (3) of Table 7 we list values that we derive for each of these parameters using our DA measurement. We know that simulation A gave slightly more absorption than we observed: 0.1287 ± 0.0027 compared to 0.118 ± 0.010 from the Kast spectra. This means that the parameters of A together with the DA measurement are not a concordant set of values. We can reduce the DA from simulation A by adjusting any one of the six parameters listed in the table. If we pick only one parameter, change it to the value given in column (3) of the table, and then rerun simulation A leaving the other parameters unchanged at the values in Table 6, we would expect to reproduce the observed DA. A concordant set of parameters comprises the values in Table 6 for simulation A, together with one, and only one, derived value from column (3) of Table 7. The Table 6 parameters for simulation A are the same as the nominal prior values in column (2) of Table 7, except for Ω_b.

The errors that we list on the derived parameters in column (3) of Table 7 are propagated from the measurement error on the DA. The errors on the derived parameters are the changes in the parameters corresponding to a change in the DA of 0.01 from the measured value. We do not combine the errors on all the parameters, because we do not know the full set of relationships between them. The derived parameters are the values we obtain using our DA measurement, using no information on the parameter in question, and assuming that all the other parameters have the values we used in simulation A, without errors.

The relative errors on the derived parameters, in column (4), are rather similar, except for γ_{228}. The DA is less sensitive to γ_{228}, and the value that we use is not a measure of the flux in the universe because we use optically thin simulations.

In column (5) of Table 7 we list $\delta\mathrm{DA} = (d\mathrm{DA}/dx)\delta x$ (except for Ω_Λ, see § 12.1.3), the change in DA in a simulation from a change in parameter x, where we use the errors from the column (2) for the δx values. For most parameters the errors on the priors give errors on the DA slightly smaller than our measurement error. The two parameters where the DA can potentially bring the most improvement in accuracy are γ_{912} and σ_8.

We now discuss how we derived each parameter and the other values in Table 7.

12.1.1. *How the DA Depends on γ_{912} and σ_8*

If we increase the UVB intensity, we reduce the amount of H I. The effect on the DA is similar to an increase in σ_8 that removes baryons from the low-density IGM where they absorb most.

In Figure 17 we show the approximate intensity of the UVB required to explain the observed DA. The vertical axis is the photoionization rate per H I atom in the low-density optically thin IGM. We use the units of the predicted rate at $z = 1.9$ from (Madau et al. 1999):

$$\Gamma_{912} = 1.329 \times 10^{-12} \gamma_{912}\ \mathrm{s}^{-1}, \tag{24}$$

where γ_{912} is a dimensionless number. Madau et al. (1999) predicted $\gamma_{912} = 1$, and when we adopt their spectrum shape, the ionization rate is proportional to the intensity of the UVB, $J_{\mathrm{H\,I}}$ (Hui et al. 2002, eq. [3]). We show how the UVB intensity required to give the DA8$s = 0.118 \pm 0.010$ for the Kast IGM

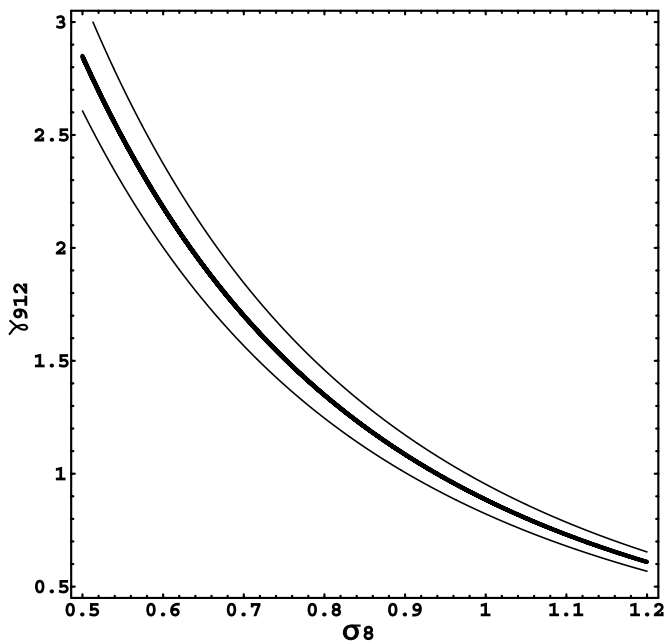

FIG. 17.—Ionization rate per H I atom in the IGM as a function of the amplitude of the matter power spectrum σ_8. The vertical axis γ_{912} is the ionization rate per H I atom, Γ_{912}, in units of the rate from Madau et al. (1999) at $z = 1.9$. When we adopt their spectrum, γ is proportional to the intensity of the radiation, J_{912}. The central curve shows the approximate γ_{912} and σ_8 values that give the DA8$s = 0.118 \pm 0.010$ that we measured in the Kast spectra for the low-density IGM only, at $z = 1.9$. The outer two curves give the $\pm 1\ \sigma$ range for the DA8s. These DA values exclude metal lines and the Lyα lines of LLSs. Models with larger γ_{912} and larger σ_8 than the curves, in the upper right, have too little H I absorption, while those below have too much. Larger γ_{912} values leave less H I and less absorption than we see. Larger σ_8 leaves fewer baryons in the IGM where we get the most absorption per baryon.

only, as a function of σ_8. We found these curves using scaling relationships that we derived from many simulations that we ran with a variety of parameters in 19.2 Mpc boxes. A smaller intensity is required when we have a larger σ_8, since there are then fewer baryons in the IGM that we need to ionize.

We obtained the derived σ_8 value in Table 7 from the central line on Figure 16 at the $\gamma_{912} = 1.0$ value that we used in simulation A. We used the same method to find the derived value for γ_{912}.

If we consider the DA alone, there is a strong degeneracy between the best-fit UVB intensity and σ_8 values. We can break this degeneracy using the variation in the DA at some z, which we can take from the power spectrum of the flux, or from $\sigma(\Delta z = 0.1)$ if we know the linear bias for the appropriate model. In T. Jena et al. (2004, in preparation) we use the power spectrum of the flux together with the DA to obtain values for σ_8 and γ_{912} separately. We can break the degeneracy because the two parameters effect simulated spectra in very different ways. An increase in γ_{912} gives a uniform decrease in optical depths, while an increase in σ_8 gives narrower Lyα lines (Theuns et al. 2000, Fig. 5).

The DA is sensitive to the power spectrum across a wide range of wavelengths. We can parameterize the power spectrum using the combination of σ_8 and the slope n at wavelengths that have the most effect on the DA. The constraints that we give on σ_8 applies to a power spectrum of slope $n = 1$. We would deduce different σ_8 for different n values (Zaldarriaga et al. 2003; Seljak et al., 2003, Fig. 1*b*; Viel et al. 2004, Fig. 8).

12.1.2. *How the DA Depends on* Ω_b

We estimate the effect on the DA of a change in Ω_b from

$$\Omega_b = 0.044(\gamma_{912}\tau_{\rm eff}/0.1378)^{1/\alpha}, \qquad (25)$$

from Gardner et al. (2003), where $\tau_{\rm eff} = 0.1378$ corresponds to the DA($z = 1.9$) = 12.87% from the simulation A with $\Omega_b = 0.044$, and we use $\alpha = 1.7$. Gardner et al. (2003) find they can keep DA constant when $\gamma_{912} \propto \Omega_b^{1.7}$. Since $\tau_{\rm eff} \propto 1/\gamma_{912}$, then $\Omega_b \propto \tau_{\rm eff}^{1/1.7}$. The exponent is 1.7 rather than 2 because larger Ω_b gives larger proper densities for fixed overdensity, and hence larger temperatures. However, changing Ω_b also changes the relative importance of Jeans smoothing, an effect ignored by Gardner et al. (2003), and more Jeans smoothing implies more absorption, much like the effect of decreasing σ_8.

If the other parameters all had insignificant errors, the $\Omega_b = 0.0417 \pm 0.0022$ that we derive from our DA measurement would be more accurate than that using our measurements of D/H: $\Omega_b = 0.042 \pm 0.004$ (Kirkman et al. 2003), and comparable in accuracy to that from the first year *WMAP* data, $\Omega_b = 0.0444 \pm 0.0018$ (Spergel et al. 2003). The DA is very sensitive to the Ω_b, but it is also sensitive to many other parameters.

12.1.3. *How the DA Depends on* Ω_Λ

We ran several simulations in flat models with $\Omega_b = 0.04$ and $h = 0.69$ to explore the effects of Ω_Λ. A model with $\Omega_\Lambda = 0.5$ gave DA = 0.12, one with $\Omega_\Lambda = 0.7$ gave DA = 0.16, and $\Omega_\Lambda = 0.9$ gave DA = 0.23. We use these values to calculate the rate of change of τ with Ω_Λ. We use τ and not the absolute DA values, since we used an unfavored γ_{912} value. Fitting a curve to τ against $y = (1 - \Omega_\Lambda)^{0.6}$, an arbitrary choice, we find $d\tau/dy = -0.31$ at $\Omega_\Lambda = 0.7$. We use $\delta\tau = (d\tau/dy)\delta y$ to calculate that a model with $\Omega_\Lambda = 0.69 \pm 0.04$ will give DA $\simeq 0.118 \pm 0.010$. An error on $\Omega_\Lambda = 0.73 \pm 0.03$, from Spergel et al. (2003) assuming a flat universe, corresponds to an error on DA of approximately 0.008, slightly smaller than our measurement error. The DA is also very sensitive to the Ω_Λ.

12.1.4. *How DA Depends on* H_0

The effect of the Hubble constant on the DA is given by equation (1): $\tau \propto h^{-1}(\Omega_b h^2)^2$. When we hold $\Omega_b h^2$ constant, τ decreases as the Hubble constant increases because there are fewer atoms per km s^{-1} along a line of sight. We have a matched pair of simulations at $z = 3$ that confirm this. One with $\Omega_b = 0.040$ and $h = 0.69$ ($\Omega_b h^2 = 0.0190$) gave DA = 0.42, while its partner with $\Omega_b = 0.030$ and $h = 0.80$ ($\Omega_b h^2 = 0.0192$) gave DA = 0.38. The predicted ratio the τ values is 1.1406, and we measure 1.1395, which agrees to within the measurement errors of approximately 1%. Our 1024^3 simulation A used $H_0 = 71$ km s^{-1} Mpc^{-1} and gave DA = 0.1287 ± 0.0027. The error on the Hubble constant from Spergel et al. (2003), $H_0 = 71^{+4}_{-3}$ km s^{-1} Mpc^{-1}, propagates to an error on DA = $0.1287^{+0.0053}_{-0.0064}$, about half the error in the measurement of the DA.

12.2. *Thermal History*

DA($z = 1.9$) depends on the history of the IGM temperature at $z < 4$. The ionization of He II to He III is especially important because it occurs over a gigayear at low redshifts 4–2 (Sokasian et al. 2002). The photoelectrons that are released when the He II is ionized heat the IGM and decrease the DA, which in turn affects the best-fit Ω_b, Ω_Λ, H_0, σ_8, and γ_{912} values. Theuns et al. (2002) discuss how a possible feature in the DA(z) might be used to identify the He II ionization epoch.

Fortunately, DA at $z = 1.9$ is insensitive to the early thermal history such as ionization of H and He I at $z > 10$. Miralda-Escudé & Rees (1994) showed that a range of histories for the early, $z > 9$, H I ionization lead to similar results at $z < 4$. This is a major reason why the thermal history is not better known. Hui & Haiman (2003) reach similar conclusions and give a formula for the late time asymptotic temperature. This temperature is a function of the shape, but not the intensity of the ionizing spectrum because increased intensity leads to decreased H I, leaving the radiative heating per baryon unchanged (Miralda-Escudé & Rees 1994; Abel & Haehnelt 1999, eq. [3]; Valageas et al. 2002, eq. [21]).

12.2.1. *Choice of* γ_{228}

We use $\gamma_{228} = 1.8$ because this supplies the heating required to match the b-value distribution at $z = 2$. This is the heating required in our optically thin simulations. The universe contains dense regions that are optically thick, and hence we would need a smaller γ_{228} value in an optically thick simulation.

In Figure 18 we compare the distributions of the b-values of Voigt profiles fitted to real spectra and to simulation B. The two appear identical within the random errors.

We obtained the real b-values from Figure 10 of KCD01, at redshifts $z = 1.61$, 1.98, and 2.13. We use their sample A, which includes lines with $12.5 < \log N_{\rm H\,I} < 14.5$ cm^{-2} and errors of less than 25% in both $N_{\rm H\,I}$ and b. The sample has 286 lines, from $1.5 < z < 2.4$, and shows no evolution. The mean redshift is 2.00.

Simulation B has parameters identical to the 1024^3 simulation A, including $\gamma_{912} = 1$ and $\gamma_{228} = 1.8$, but it has 256^3 cells in a 9.2 Mpc box, giving a resolution of 37.5 kpc resolution, twice that of our 1024^3 simulation. The two simulations give the same DA values, but simulation A gives b-values that are 15% larger because of numerical smoothing.

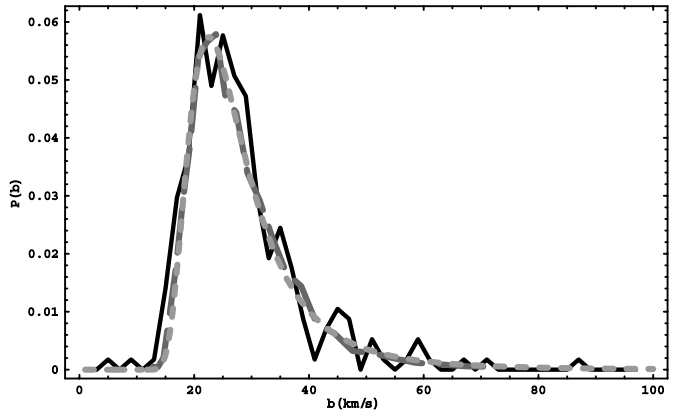

FIG. 18.—Probability distribution of b-values of Voigt profiles fitted to Lyα lines with $12.5 < \log N_{\rm H\,I} < 14.5$ cm^{-2} at $z = 2$. The vertical axis has units of lines per km s^{-1}. The jagged solid dark line shows the data from KCD2001 (sample A, Fig. 10) for $1.5 < z < 2.4$, in 2 km s^{-1} bins centered on odd integers. The highest point shows that 35 of the 286 lines, or 0.122, have $20 < b < 22$ km s^{-1}. The lighter long dashed lines show the lines from simulation B at $z = 2$. The faint short dashed lines show a fit to the simulation B distribution using $b_\sigma = 23.8$ km s^{-1} that is indistinguishable from the simulation except near 40 and 50 km s^{-1}. All three distributions have unit area.

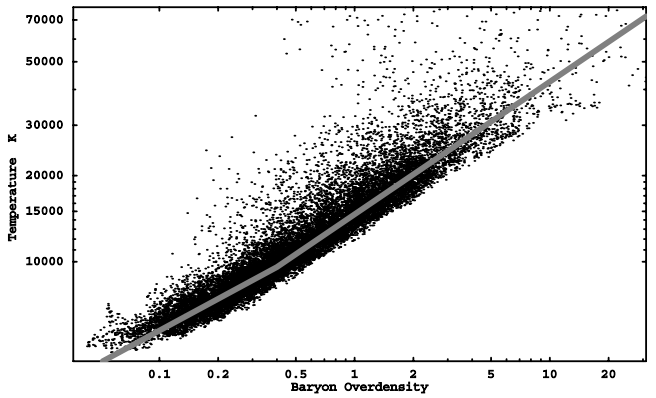

FIG. 19.—Temperature as a function of the baryon density at $z = 2$ in the cells of the hydrodynamic simulation B. The line shown is a double power law, specified in Table 8.

We compare the b-value distributions for the simulations to that from QSO spectra using the fitting formula (KCD01, eq. [3])

$$dn/db = B_{\rm HR}\,\frac{b_\sigma^4}{b^5}\,\exp\left(-\frac{b_\sigma^4}{b^4}\right), \tag{26}$$

from Hui & Rutledge (1999), where dn/db is the number of lines per km s^{-1} and we can use b_σ to describe the velocity of the peak of the function, since $b_{\rm peak} = 2^{1/2} b_\sigma 5^{-1/4} = 0.9457 b_\sigma$.

We compare distributions using b_σ because this statistic will be relatively insensitive to the many differences between the real and simulated spectra. The simulations are optically thin with limited spatial resolution, and the simulated spectra have no photon noise, no metal line contamination, no flux calibration errors, and no continuum fitting errors. Different algorithms were used to fit the Voigt profiles to the QSO spectra and the simulations, and they will fit blends in different ways, leading to different numbers of lines with large b-values.

We use $\gamma_{228} = 1.8$ in our main simulations because this gives a b-value distribution and b_σ values similar to the data. The b_σ values are 23.6 ± 1.5 km s^{-1} for the KCD01) data and 23.8 ± 0.3 km s^{-1} for simulation B. We have not measured the systematic error, or the offset coming from the differences between the real and simulated spectra, but we guess that these values are of order 1 km s^{-1}. Later in § 12.2.3 we use an upper limit of $b_\sigma + \delta b_\sigma = 25.4$ km s^{-1}, where $\delta b_\sigma = 1.8$ km s^{-1} is the quadratic sum of the random error, 1.5 km s^{-1} and the 1 km s^{-1} guessed systematic error.

12.2.2. *Temperature-Density Relationship*

The thermal history that we used can be reproduced in numerical simulations that use the same parameters, especially the Madau et al. (1999) radiation field as a function of redshift, and the ratio of the γ_{912} and γ_{228} parameters that change the spectrum shape.

In Figures 19 and 20 we show the temperature and density for cells in the 256^3 simulation B at $z = 2.0$, 3.0.

In Table 8 we list values that describe the thermal history of the IGM in simulation B, including fits to the temperature density relation using two power laws, the temperature at the mean baryon density, and DA(z) values. We fit the ridge line of the cool gas in the temperature-density plane using two power laws, since the relationship is not a single power law (Schaye et al. 1999, Fig. 1; McDonald et al. 2001, Fig. 1). Each power law has parameters

$$T(\rho) = T_0(\rho/\overline{\rho})^\alpha, \tag{27}$$

where ρ is the baryon density, T_0 is the temperature of the baryons at the mean baryon density, $\overline{\rho}$, and we use α in place of the usual $\gamma - 1$ since we are using γ for the ionizing flux. We list two sets of T_0 values, one for each of the power laws. The values $T_0(z = 2) = 14{,}261$ K and $T_0(z = 3) = 15{,}942$ K apply to the fits for $0.2 < \rho/\overline{\rho} < 10$, and they are our best estimates of the temperatures at the mean density, $\rho = \overline{\rho}$. The second set of smaller temperatures are extrapolations of the fits to the lower density regions of the simulation.

The temperatures that we find are probably the most accurate yet obtained at $z = 2$ for an optically thin simulation, since we have an excellent fit to the entire b-value distribution in a high-resolution large simulation that fits the DA and uses modern values for the cosmological parameters. Our T_0 values are a lot higher than those in the simulation of Davé et al. (1999, Fig. 11), who had $T_0 \simeq 9000$ K. Our temperatures are lower than the measurement of $T = 22{,}600 \pm 1900$ K at $1.66\,\overline{\rho}$ and $z = 2.4$ from McDonald et al. (2001). For comparison we have $T(1.66\,\overline{\rho}) = 19{,}600$ K at $z = 2.0$ and $T(1.66\,\overline{\rho}) = 20{,}700$ K at $z = 3.0$. Our temperatures are very similar to the $T_0(z = 2) = 15{,}000$ and $T_0(z = 3) = 17{,}000$ K from the semianalytic

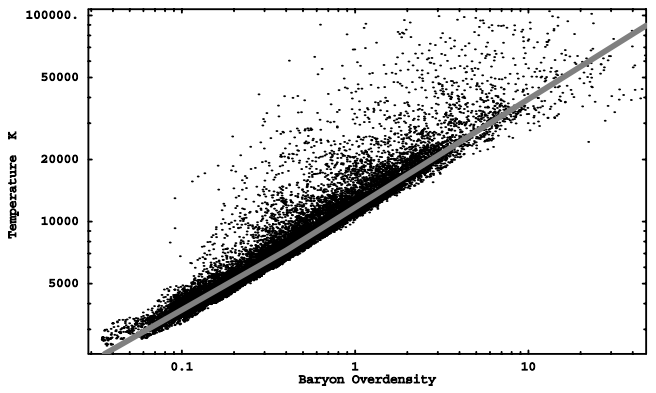

FIG. 20.—As Fig. 19, but for $z = 3$.

TABLE 8
THERMAL HISTORY OF THE IGM IN SIMULATION B

	$\rho < 0.2\overline{\rho}$		$\rho > 0.2\overline{\rho}$	
z	T_0 (K)	α	T_0 (K)	α
2.....	11270	0.4705	14261	0.6260
3.....	13103	0.3318	15942	0.5137

stochastic models of Hui & Haiman (2003, Fig. 6). The Eulerian code that we use to simulate the IGM gives volume weighted mean temperatures that may differ from the mass weighted temperatures that come from often used smoothed particle hydrodynamics simulations.

Simulations with three-dimensional radiative transfer (Abel et al. 1999; Bolton et al. 2004; Ciardi et al. 2003a, 2003b; Gnedin & Abel 2001; Nakamoto et al. 2001; Razoumov et al. 2002; Sokasian et al. 2001, 2002, 2003a, 2003b) will give more realistic mean temperatures and distributions for the temperature at each density. Bolton et al. (2004) have run a simulation that includes radiative transfer effects for H and He. They find that, compared to an optically thin simulation, the gas becomes much hotter when it is ionized. There is also a range of temperatures for a given low density. The range comes from the different shapes of the UVB spectrum at different places in the simulation. It also comes in part from the ionization of different places at different times. Over time the gas cools adiabatically, with the low-density regions cooling faster. In a model with a QSO source inserted at $z = 6$, a wide range of higher temperatures remain at $z = 3$, and the gas is hotter than in the optically thin case, especially at the lowest densities. However, by $z = 1$ there is a single temperature for a given density, and this temperature is only slightly higher than for the optically thin case.

Our optically thin simulation may have α-values that are too large. Our simulation has too low a temperature at $z = 2$ compared to a simulation with radiative transfer. To compensate and match the observed b-values, we increased the heating by increasing γ_{228}. However, this change is not sufficient to correct the temperature density relation. Bryan & Machacek (2000, Fig. 4) show that increasing γ_{228} gives a slightly smaller α where as the simulations with radiative transfer can have much smaller α-values long after ionization (Bolton et al. 2004).

We do not know how much the DA would differ in a simulation with radiative transfer that matched the b-value distribution. However, the effects will be less at $z = 2$ than at higher redshifts.

12.2.3. *Range of Allowed Thermal Histories and γ_{228}*

There may be other models for the IGM that also fit the data at $z \simeq 1.9$. Some of these models might have different thermal histories, while others might also have different cosmological parameters. We have not explored these models because this is a large task. For example, we should compare these models with the full set of IGM data on He II as well as H I.

However, we have examined the effect on the DA of the temperature at $z = 2$. The temperature effects the DA in two competing ways. The dominant effect is to change the recombination rate. Higher temperatures give smaller values of DA. Higher temperatures also inhibit the clumping of the gas, Jeans smoothing, and this tends to increase the DA, as does smaller σ_8.

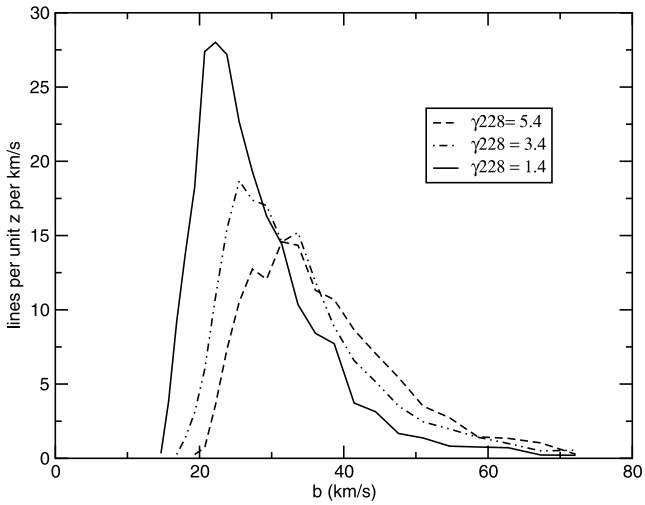

FIG. 21.—Distribution of b-values of Voigt profiles fitted to lines in artificial spectra from hydrodynamic simulations C, D, and E at $z = 2$. The simulations are identical except that they had three different values for the rate of ionization of He II, labeled by $\gamma_{228} = 1.4$, 3.4 and the highest rate, 5.4. The b-values are slightly enhanced by numerical smoothing. Higher γ_{228} values produce more heating and larger b-values. The vertical axis is the number of lines fitted per unit redshift for Lyα, per km s^{-1}. The b-values are distributed in bins with centers given by $b = 22.20472 \times 1.07177^n$ km s^{-1}, where n is a whole number. The number of lines that we count in each bin is 10 times the values shown, because we made 100 artificial spectra, each of length $\Delta z = 0.1$.

We ran three simulations, C, D, and E each with a different thermal history. The simulations each had 256^3 cells and 75 kpc resolution, the same as the 1024^3 simulation A. The other parameters were the same as simulation A, except that to save time we used $\sigma_8 = 0.94$ and $\gamma_{912} = 1.2$, values that were built into the simulation software. Simulations C, D, and E each use a different value for γ_{228} to vary the amount of heating.

In Figure 21 we show the distributions of the b-values for simulations C, D, and E at $z = 2$. The b-values are too large, because the simulations had a factor of 2 lower resolution than we need for convergence. However, they suffice to help us estimate the change in the DA with γ_{228}. The entire distribution moves to larger b-values as the γ_{228} increases. (Theuns et al. 2000, Fig. 6) show a figure for $z = 3$ that is similar except that they changed their γ_{912} factor to conserve the DA. They demonstrate that the changes are from the combined effects of thermal broadening, pressure-induced peculiar velocities and Jeans smoothing that makes the absorbing regions larger and experience more Hubble flow. The area under the distribution in our Figure 21 decreases with increasing γ_{228} because the number of lines decreases. The change in the DA is less because one partly saturated line with $b = 40$ km s^{-1} causes more absorption than one with $b = 20$ km s^{-1}.

In Table 9 we list fits to the b-value distributions and the mean DA for the low-density IGM in simulations C, D, and E at $z = 2.0$. We made 100 artificial spectra through each simulation, and we fitted Voigt profiles to the Lyα lines in each using the code described in Zhang et al. (1997). Each spectrum started in a random direction and wrapped through the box several times to accumulate a length of $\Delta z = 0.1$. By design, simulation C has the same $b_\sigma = 23.8$ km s^{-1} as simulation B. We used a lower $\gamma_{228} = 1.4$ for C to adjust for its lower numerical resolution and larger σ_8 value compared to A.

The variation of γ_{228} has a large effect on both the temperature and the b-value distribution, but a relatively small effect on the DA value.

TABLE 9
Fits to b-values for Simulations with Different Thermal Histories

Simulation	γ_{912}	γ_{228}	b_σ (km s^{-1})	DA
C	1.2	1.4	23.8	0.1071
D	1.2	3.4	28.8	0.0898
E	1.2	5.4	31.9	0.0812

We estimate the uncertainty in the DA from the uncertainty in the b_σ using

$$\delta \mathrm{DA} = \frac{d\mathrm{DA}}{db_\sigma}\delta b_\sigma, \tag{28}$$

where $d\mathrm{DA}/db_\sigma = -0.0034\delta b$, from the first two rows of Table 9, or -0.0030 from the second and third rows, and we use $\delta b_\sigma = 1.8$ km s^{-1} from § 12.2.1, giving $\delta \mathrm{DA} = 0.006$, which is 60% of the error in our measurement of the DA. We conclude that uncertainty in the temperature at $z = 2$ is not the dominant error in the interpretation of our DA measurements.

We use γ_{228} to adjust the temperature of a simulation, to match the b-value distribution. The range of γ_{228} allowed by the b-values corresponds to a small range in DA, too small to allow us to match the observed DA with $\gamma_{228} > 1.8$. To reduce the DA of the simulation from 0.1287 to 0.118 we would need a simulation with $\gamma_{228} \simeq 3.2$. If we leave other parameters, such as σ_8 unchanged, this would give $b_\sigma \simeq 27$ km s^{-1}, which is noticeably larger than that of the data. The 1 σ upper limit on γ_{228} is approximately 2.4, since simulations C and D suggest, very roughly, that this γ value would give $b_\sigma \simeq 25.4$ km s^{-1}, the 1 σ upper limit we gave in § 12.2.1.

The b-values of the simulation can also be changed by both σ_8 and the way in which the gas is heated. The effect of σ_8 is discussed by Hui & Rutledge (1999), Bryan & Machacek (2000), Theuns et al. (2000), and Schaye et al. (2000). Theuns et al. (2000, Fig. 5) show that models with smaller σ_8 values and larger γ_{912} to conserve the DA, had wider absorption features. If we use smaller σ_8 values for the simulations, we would need lower temperatures to match the b-values of the QSO spectra. Unfortunately, the changes in the simulated spectra may be missing from the b-value distribution. The absorption line profiles become more complex, less Voigt in shape, and a spectrum can be fitted using additional components instead of wider lines. The VPFIT code used by Theuns et al. (2000) and KCD01 fits additional components that leave the peak of the b-value distribution little changed when σ_8 is decreased.

The effect of the heating on the b-values is unclear. Bolton et al. (2004) show that radiative transfer leaves some places, especially in the low-density regions, at very high temperatures. The injected energy per photoionization undergoes a large boost when high-energy photons leak beyond the ionization fronts to heat the gas before it is ionized. We do not know what this will do to the b-value distribution. The effects might be hard to detect, as is the case for feedback from galaxies. Cen et al. (2004) find that Galactic Superwinds do not make noticeable differences to the b-value distribution.

12.2.4. *Parameters Derived from the DA*

The values in Table 7 show that our measurement of the DA is accurate enough to give significant new cosmological information. This information is difficult to extract because the DA depends on at least six parameters. We would need to know all the other parameters to derive an unknown using the DA alone. We need to explore a six dimensions space to find the best concordance model, and to find the full errors on derived parameters. Hydrodynamic simulations on modern supercomputers are now up to this task that has become practical because we now have accurate prior measurement for the parameters.

The values collected in Table 7 show that the changes required in five of the six parameters of simulations A to match the observed DA are modest. The exception is γ_{228} because the DA is insensitive to this parameter. Column (4) lists the relative error on the derived values, σ(derived value)/(derived value). This is a measure of the sensitivity of each parameter to the DA. The DA is most sensitive to σ_8, Ω_b, and Ω_Λ. It is less sensitive to γ_{912}, H_0 and especially γ_{228}.

Column (5) of Table 7 gives the change that we expect in the DA if we change a parameter by the 1 σ error on the listed prior measurement. For two parameters, H_0 and γ_{228} we would need to change the parameter by approximately 2 σ to reduce the simulation A DA value to the measured value. For γ_{228} this change is excessive.

The uncertainties on the prior measurement of the six parameters lead to errors on the DA that have a factor of 5 range. The logarithmic mean of this range is similar in size to the error on our measurement of the DA. The DA responds to cosmological parameters much as do other observable quantities. It is not surprising that the DA depends on all six parameters, since these are the set required to model the universe in general, with the addition of the two γ parameters for the IGM. These six parameters provide a realization of equation (1).

Our DA value gives γ_{912} to higher accuracy than has been possible before, since the error of 0.1 on γ_{912} from Madau et al. (1999) seems optimistic and the proximity effect gives larger errors (Liske & Williger 2001; Scott et al. 2002). We find $\gamma_{912} = 1.08 \pm 0.27$ or $\Gamma = (1.44 \pm 0.36) \times 10^{-12}$ s^{-1}, where the error now includes the contributions from the errors on Ω_b, σ_8 and DA. Using equation (3) of Hui et al. (2002), this Γ_{912} value corresponds to an intensity of the UVB $J_{\mathrm{H\,I}} = 0.33 \pm 0.08 \times 10^{-21}$ ergs s^{-1} cm^{-2} Hz^{-1} sr^{-1}. The main contribution to this error is from the uncertainty in σ_8. We illustrated this in Figure 16. We do not include the contributions to the error from Ω_Λ, H_0, and γ_{228} because we do not know how these parameters are correlated with the others. However, from Table 7, they appear to add little to the total error on γ_{912}.

13. SAMPLE SIZE, SPECTRAL RESOLUTION, LLS, AND METALS

The asymmetric DA distribution extends to scales greater than 153 Mpc. There remain correlations in the Lyα absorption from the IGM, from the matter power spectrum on large scales. The metal lines are correlated because one system can create lines all over a spectrum. The DA distribution is also asymmetric because the Lyα lines of DLAs are rare events that produce huge DA values.

The σ decrease more slowly than $(\Delta z)^{-0.5}$, as we discussed in § 11.1. When we take the mean of 152 DA2s values from Table 4, we would expect the $\sigma = 0.0612/\sqrt{152} = 0.50\%$ if the DA2s values were uncorrelated. Instead we find a larger value, $\sigma(\mathrm{DA3}s) = 0.64\%$, from the Kast measured column of Table 5.

To help us compare measurements from different samples, we can use a first order estimate

$$\sigma(\mathrm{DA}s, z = 1.9) = 0.024(\Delta z)^{-0.4}, \tag{29}$$

where Δz is the path length in the sample at $z = 1.9$, and the coefficient and power are from a straight line fit to the $\sigma(\mathrm{DA3}s)$ from the quarters of the Kast the sample (Table 5) and $\sigma(\mathrm{DA2}s)$ from the $\Delta z = 0.1$ (Table 4). This σ is for DA values that include metal lines and the Lyα of LLSs. Each QSO contributes a maximum of $\Delta z = 0.156(1 + z_{\mathrm{em}})$ when we use all wavelengths from Lyβ to Lyα, and, for our sample, typically around 0.6 of this or $\Delta z = 0.3$ at $z = 1.9$.

We expect to obtain approximately the same $\sigma(\mathrm{DA})$ with 4 times smaller Δz when we use spectra that are free of both the metal lines and the Lyα from LLSs. Our estimate that the $\sigma(\mathrm{DA2}s) = 0.039 \pm 0.006$ implies that we might achieve

$$\sigma(\mathrm{DA}) = 0.012(\Delta z)^{-0.5} \qquad (30)$$

with such spectra. This suggests that we might obtain an error on DA8s (IGM only) of 0.01 with only five high-resolution spectra, comparable to the error we obtained with the 77 Kast spectra, after we removed the mean absorption by LLSs and metal lines. However, we would need improvements in the flux calibration and continuum fitting to echelle spectra to obtain errors in the DA of 0.01. Suzuki et al. (2003) found it very difficult to obtain such small errors, using purpose built software, and with ample calibration spectra.

14. COMPARISON WITH PRIOR MEASUREMENTS AND DA AT HIGHER REDSHIFTS

The few prior estimates of the DA at $z = 1.9$ all involve small samples and they are all compatible with our new measurements.

KCD01 (Fig. 15) show measurements from about 11 QSOs near that z, with a mean DA of about 10% and a range of 6%–15% that includes the values from the Kast spectra. They fit a power law to τ_{eff} values from UVES and HIRES spectra that include Lyα lines of LLSs, but no DLAs or metals, giving DA = 10.9 % at $z = 1.9$. Our equivalent value, between the values for DA7s and DA8s, is approximately 12%.

Rauch et al. (1997) measured the DA in seven HIRES spectra. They identified and rejected metals and all lines with $b < 10$ km s^{-1}. At $z = 2.0$ they found DA = 14.8%, with no error offered. Since only two QSOs contributed data at $z < 2.3$, we estimate their error is greater than 1.6% (eq. [30]). Our equivalent value, DA7s = 12.8% ± 0.9%, is smaller.

Schaye et al. (2003) present a measurement of DA from high-resolution UVES and HIRES spectra of 21 QSOs, with 6.6 km s^{-1} resolution, seven of which contribute at $z = 1.9$ %. Their best fit (Fig. 1) gives DA(1.905) = 12.6%, or 10.9 % after they remove metal lines and Lyα lines from systems with $\log N_{\mathrm{H\,I}} > 19$ cm^{-2}. Our equivalent value is approximately 12% ± 1%, and it is larger, but not significantly.

14.1. *A Possible Event in the Evolution of the Ionization of* H I

In Figure 22 we show as a function of redshift the DA measurements from MW04 (Table B1) that are on a consistent statistical basis. We also show our measurements and simulation results, and the results from B03. There are at least three ways to interpret this interesting plot because the DA values at $z > 2.4$ are inconsistent. We note one major inconsistency and two minor ones.

B03 report systematically more absorption than the values derived by MW04 from PRS93 and SS87). The DA values in all three cases include all absorption in the Lyα forest,

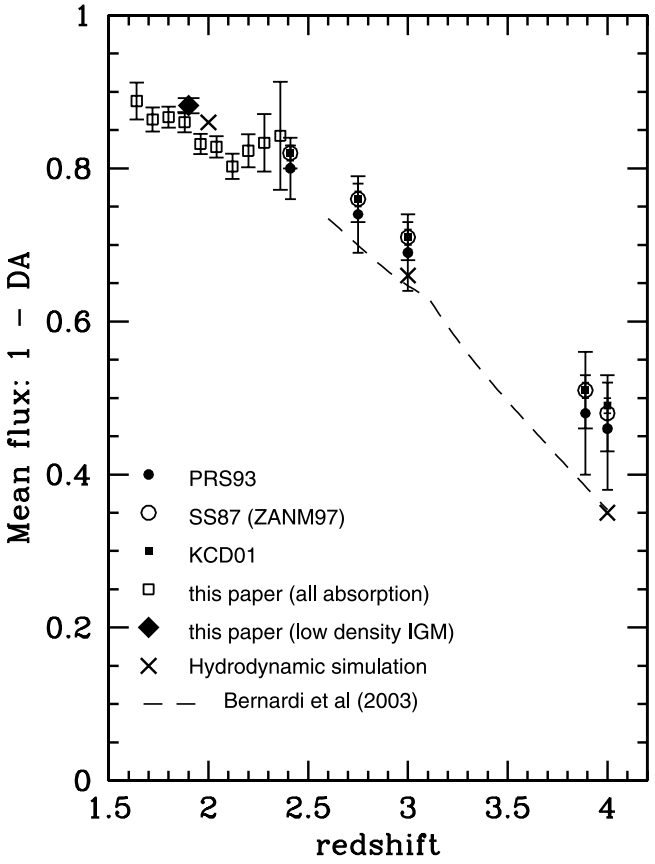

FIG. 22.—Mean flux in the Lyα forest as a function of absorption redshift for Lyα. The 10 open squares on the left are our total DA values (including Lyα lines of the LLS, DLAs, and metal lines) from Table 2. The filled diamond is our DA value, 11.8 ± 1.0%, for the low-density IGM alone. The crosses without error bars are the DA values from the 1024^3 hydrodynamic simulation A for the low-density IGM at redshifts 2, 3, and 4. The other values are estimates from MW04, Table B1, with their Monte Carlo generated effective 1 σ error bars. The filled circles are values derived from PRS93, who use spectra from Schneider et al. (1991) of 33 QSOs that include metal lines, Lyα of LLSs and about six candidate DLAs. Open circles are data from SS87, fitted by Zhang et al. (1997). These values also include metal lines and the Lyα lines of LLSs, although there were no DLAs. Small squares are values from KCD01 that are coincident with those from SS87 except at $z = 4$. For HIRES spectra KCD01 use line lists, and they exclude the metal lines and DLAs, but they include the Lyα of non-DLA LLSs. For UVES spectra they used the flux in the spectra rather than the line lists, and again they included "high column-density absorption systems" (LLSs, not DLAs). Zhang et al. (1997) found that the mean optical depth from line lists differed from the values from spectra by less than 0.03 for $1 < z < 3$, while KCD01 comment that in their experiments there was no "noticeable difference."

including the Lyα lines of LLSs and DLAs and metal lines, and hence all three should be the same.

There is a minor difference between SS87 and PRS93. The DA values from SS87 are systematically smaller than those from PRS93, by 0.02–0.03 at all five redshifts. This may be due in part to the inclusion of DLAs in the PRS93 analysis that are not present in the SS87 data.

There is also a minor inconsistency between the DA values from KCD01 and the values from SS87. The values are identical at four redshifts, and yet we would expect SS87 to show more absorption because they include metals while KCD01 do not. We estimated that the metal lines have DM = 2.3% ± 0.5% at $z = 1.9$, and we expect more metal lines at higher z, because there is more path length to the QSOs and more LLSs and DLAs per unit z at higher z. Both of the minor inconsistencies would be resolved if the SS87 DA values were

increased by approximately 0.03, smaller than the estimated errors on the SS87 points.

The first way to interpret the plot is to compare the DA values that include all absorption in the Lyα forest, including the Lyα lines of LLSs and DLAs and metal lines. We compare our 10 values from Table 2 at $z < 2.4$ with values at $z > 2.4$ derived by MW04 from PRS93 and SS87. The data analyzed by MW04 have DA $= 0.18 \pm 0.02$ at $z = 2.41$ that joins smoothly with our values near $z = 2.3$. Comparing these values, we see that the DA at $z = 2.1$ is similar to the value at $z = 2.4$. It appears as if the DA stopped evolving, which is very different from the trends at both $z < 2.1$ and $z > 2.4$. The three DA values that we measured at $1.9 < z < 2.1$ appear to make a dip in DA(z) with more absorption than we might expect from a smooth extrapolation of the values at $2.4 < z < 3$ from PRS93 and SS87.

Second, our DA at $z < 2.1$ is approximately consistent with a smooth extrapolation of the B03 values, perhaps with a period of exceptionally low DA that appears as a peak in Figure 22 at $2.1 < z < 2.3$. We do not prefer this interpretation because our three values each have large random errors, and the values from B03 are systematically lower than those from PRS93, SS87 and KCD01.

Third, we can compare our DA value at $z = 1.9$ for the low-density IGM alone with the KCD01 values that are for the low-density IGM plus the Lyα lines from LLSs, but not from DLAs. All six DA values can be connected by a smooth featureless curve.

The first interpretation of Figure 22 accepts the DA from PRS93 and SS87 but not B03. It implies a sudden change in the evolution of the amount of absorption in the Lyα forest at redshifts near $z = 2.25$. This might come from a reduction in the intensity of the UVB at $z < 2.4$ that leaves the IGM less ionized than we expect from the data at $z > 2.4$. At redshifts 2.1–2.4 the reduction in the UVB might approximately cancel the increase in the ionization driven by the expansion of the universe. This is the standard explanation for the slow decline in the number of Lyα lines seen in *HST* spectra per unit z at $z < 1.6$ (Theuns et al. 1998; Davé et al. 1999).

The second interpretation accepts the B03 values and requires that the DA values from PRS93 and SS87, and probably also KCD01 are all too small. The possible period of low DA might then be a time of increased ionization at $2.1 < z < 2.3$. The physical origin might be the ionization of He II to He III that releases hot electrons that increase the ionization fraction of hydrogen through a reduced recombination rate. Theuns et al. (2002) used the same physical event to explain the order of magnitude smaller dip in the DA that B03 reported at $z = 3.2$.

The third interpretation alone does not require any unusual evolution of the ionization. It could be consistent with the second interpretation if there is no dip in the DA at $2.1 < z < 2.3$ and if the DLAs and metal lines caused enough absorption to explain the difference between the KCD01 and the B03 values.

In Figure 22 we also show the DA values for the low-density IGM from the hydrodynamic simulation A: 0.1339 at $z = 2$, 0.3434 at $z = 3$ and 0.6455 at $z = 4$. These DA values have errors of order 0.5% from the numerical resolution of the simulation and the number of artificial spectra that we used to make the measurements.

Simulation A fits a variety of data (DA, power spectra, line widths, and the UV background calculation) at $z \simeq 1.9$, but it appears to have too much H I absorption at $z > 3$, since we think it is unlikely that the B03 values are correct and that there is negligible absorption at $z = 3$ and 4 from both the Lyα lines of LLSs and metal lines. We could reduce the absorption in the simulation by increasing the flux of UV radiation that ionizes hydrogen at $z = 4$. This probably means that the UVB is more intense than calculated by Madau et al. (1999), perhaps containing more radiation from hot stars. Our simulation underestimates the amount of H I absorption because it is optically thin. An optically thick simulation would show more absorption, and hence to match the data it would need a still higher intensity for the UVB, from hot stars or a higher rate of ionization by QSOs (MW04).

15. DISCUSSION AND SUMMARY

We have measured the amount of absorption in the Lyα forest in spectra of 77 QSOs from the Kast spectrograph on the Lick 3 m telescope. We measured the mean amount of absorption and the contributions from the Lyα lines of LLSs and metal lines. We also measured the variance in the amount of absorption from the metals, the LLSs and the Lyα in the lower density IGM. The amount of absorption that we find is consistent with that in a large hydrodynamic simulation that uses popular values for the cosmological and astrophysical parameters. We summarize this work under these three topics and discuss opportunities for improvements.

15.1. *Mean DA*

We fitted continua to the Kast spectra and to artificial spectra that we made to mimic them. The relative error in our continuum fits to the artificial spectra is 3.5% on average. The mean from all 77 spectra is within 1%–2% of the correct value, except when the S/N per 1.13 Å pixel is less than 6, where we systematically placed the continuum too high. We corrected this systematic bias and also our tendency to place the continuum 0.5% too high where there is a lot of absorption.

We find that the total absorption in the Lyα forest between 1070 and 1170 Å at $z = 1.9$ is DA $= 0.151 \pm 0.007$, including absorption by metal lines and the Lyα lines of LLSs (defined to include all DLAs). This is the first measurement of the DA to be made at any z using a calibrated continuum fitting procedure, and the first of any sort using a large sample at $z \simeq 2$.

We measured the mean absorption due to metals at 1225–1500 Å in both our 77 Kast spectra and from the lists of absorption lines in 26 spectra in Sargent et al. (1988). The results agree. Near $\lambda_r = 1360$ Å, DM3 $= 0.0187 \pm 0.0013$ from our Kast spectra and DM4 $= 0.0167 \pm 0.0022$ from SBS88.

We must extrapolate the DM to obtain the metal absorption in the Lyα forest, and this increases the uncertainty. The extrapolation gives DM1 $- 6(1120) = 0.0192 \pm 0.0042$, and we increase this by a factor of 1.2 to account for extra metal lines in the Lyα forest, giving DM$s = 0.023 \pm 0.005$.

The total absorption in rest wavelengths 1070–1170 Å comprises: DA6$s = 0.010 \pm 0.004$ from LLSs, DM$s = 0.023 \pm 0.005$ from metals and DMA8$s = 0.118 \pm 0.010$ from the Lyα in the low-density IGM that excludes Lyα lines with $N_{\rm H\,I} > 17.2$ cm^{-2}.

The absorption from metals is important. At $z = 1.9$ the metal lines make 15% $\pm$ 4% of the total absorption and 19% $\pm$ 5% of the absorption by just the Lyα with $\log N_{\rm H\,I} < 17.2$ cm^{-2}. We have calculated the amount of absorption due to C IV alone, which increases slowly as $z_{\rm abs}$ drops, and hence λ_r for a given QSO sample. By $\lambda_r = 1120$ Å at $z = 1.9$ C IV gives DM7 $=$ 0.0080 that is 35% of the metal line absorption.

We calculated the absorption by the Lyα lines of LLSs, using a list of rest equivalent widths from other Kast spectra, and normalizing to the LLSs density seen in *HST* spectra. We find DA6$s = 0.010 \pm 0.004$, where the error is nearly all from the uncertain density of LLSs at these low redshifts and the suffix "s" refers to a value for $z = 1.9$. We calculated that the DLAs alone have DA $= 0.0085 \pm 0.0017$, which is a larger proportion of the DA6s for all LLSs than we expected. Perhaps the DA6s value is too small.

15.2. *Dispersion of DA Values*

We have measured the dispersion in the mean DA on large scales. We defined DA2s to be the mean DA in segments of a spectrum of length $\Delta z = 0.1$, or 121.567 Å in the observed frame. This is 153 comoving Mpc at $z = 1.9$. We scale the measurements to the amount of absorption expected at $z = 1.9$ since the evolution is significant. We find $\sigma(\mathrm{DA2}s) = 0.0612 \pm 0.0035$. This is a measure of the amount of power in the flux distribution on scales similar to 153 Mpc; however, it includes the power due to the Lyα of LLSs and the metal lines and the power in the error in the continuum fits.

We have estimated the dispersion in the DA2s from the Lyα lines of LLSs by making mock spectral segments of length $\Delta z = 0.1$. We added random samples of measured W_r values to the segments. We find $\sigma(\mathrm{DA2}s,\ \mathrm{LLS}) = 0.035 \pm 0.005$, much larger than the mean value of 0.010 ± 0.004. We also derived this σ analytically.

We have measured the dispersion in the amount of metal absorption in the Kast spectra: $\sigma(\mathrm{DM3}) = 0.025$. We found a similar value from the SBS88 spectra: $\sigma(\mathrm{DM4}) = 0.027$. These are the measured standard deviations of the DM values in spectral segments of $\Delta z = 0.1$, at $z = 1.9$ and $\lambda_r = 1360$ Å, which is near $\lambda_o = 4130$ Å.

We have estimated the dispersion that we expect from the metal lines in the Lyα forest. We scale from $\sigma(\mathrm{DM3}, \lambda_r = 1360) = 0.025$, to obtain $\sigma(\mathrm{DM}s) = 0.031$. Since this value is an extrapolation, its error is large and not well known. It appears to be larger than the mean DMs value, 0.023 ± 0.006.

Our measured value for the dispersion of the mean DA in segments of spectra 121.567 Å long, from the absorption in the low-density IGM alone, is $\sigma(\Delta z = 0.1) = 0.039^{+0.005}_{-0.007}$. This value includes the dispersion from the error in continuum fits that is not well known. We are able to detect the power on large scales because the Kast spectra and the continua that we fit are more stable over these large scales than are high-resolution echelle spectra and their continua (Suzuki et al. 2003). The $\sigma(\Delta z = 0.1)$ value that we measure is very similar to the value that we calculated using $\sigma_8 = 0.9$ and $n = 0.95$ in § 9.3, $\sigma(\Delta z = 0.1) = 0.0386$, although both the measurement and the calculation could have large errors.

The dispersion of the DA measured in segments of spectra 121.567 Å long in the observed frame at $z = 1.9$ for Lyα comes about equally from the low-density IGM, LLSs and metal lines.

The flux field is significantly different from a random Gaussian field, with an enhanced probability of a large amount of absorption, on all scales 10–10,000 km s^{-1}. On small scales the asymmetry comes from the density distribution in the low-density IGM, making spectra that are largely absorption free, with occasional Lyα lines. On large scales the asymmetry comes from the rare high-density regions that make absorption with large H I column densities. They make LLSs and DLAs with strong Lyα lines, and they place many strong metal lines all across a spectrum.

15.3. *Comparison with Hydrodynamic Simulations*

The mean DA that we measure for the Lyα from the low-density IGM provides a joint constraint on four cosmological parameters, Ω_b, Ω_Λ, H_0, and σ_8, and two astrophysical parameters, Γ_{912} and Γ_{228}. We assume a flat universe and an initial power spectrum index $n = 1$ to simplify the problem.

We find that an optically thin hydrodynamic simulation on a 1024^3 grid in a 75.7 Mpc box reproduces the observed mean DA from the IGM alone when we use popular parameters $H_0 = 71$ km s^{-1} Mpc^{-1}, $\Omega_b = 0.044$, $\Omega_m = 0.23$, and $\Omega_\Lambda = 0.73$, $\sigma_8 = 0.9$ and a UV background with an ionization rate per H I atom of $\Gamma_{912} = (1.44 \pm 0.11) \times 10^{-12}$ s^{-1} that is $\gamma_{912} = 1.08 \pm 0.08$ times the value calculated by Madau et al. (1999) with 61% from QSOs and 39% from stars. Our result is similar to the $\Gamma_{912} > 1.5 \times 10^{-12}$ s^{-1} from Steidel et al. (2001) at $z \simeq 3$. The error on Γ_{912} of 0.11 is from our measurement error on the DA assuming negligible errors on all other parameters. This error increases to $\Gamma_{912} = (1.44 \pm 0.36) \times 10^{-12}$ s^{-1}, when we include the contributions from the errors in Ω_b, σ_8 and the DA, but not H_0, γ_{228}, or Ω_Λ. The baryon density that accounts for the DA in the IGM at $z = 1.9$ is the same as the value measured using D/H and the CMB, within the errors.

A measurement of the variation of the DA at fixed redshift, from the flux power, or from the $\sigma(\Delta z = 0.1)$ given in § 15.2, breaks the degeneracy between the σ_8 and γ_{912} that we show in Figure 16. When we pass multiple lines of sight through the hydrodynamic simulation, we see slightly less variation in the DA in $\Delta z = 0.1$ than we did in the Kast spectra from the low-density IGM, in part because the box lacks large-scale power. In T. Jena et al. (2004, in preparation) we show that the power of the flux in these lines of sight does match that in HIRES spectra on scales $0.008 < \log k < 0.08$ (s km^{-1}).

15.4. *Opportunities for Improvement*

The values in Table 5 suggest that we could improve the accuracy of our mean DA4 measurement by observing many more QSOs, even without any improvements in the methods. The measurement error for the Kast spectra (col. [5]) would approach that from the S/N and continuum fits (col. [4]) with a sample about 4 times larger, or 300 QSOs. The values given here are approximate, since they assume that the artificial spectra are an adequate representation of the IGM, even though they do not explicitly include absorption from high $N_{\mathrm{H\,I}}$ lines and metal lines.

We find that S/N = 6 per 1.13 Å in the observed frame is adequate for continuum placement on Kast spectra at $z = 1.9$. Improved continuum placement methods might allow us to use lower S/N, but we would not be able to adjust the continua to fit the emission lines of each QSO, which would complicate measurements, especially of large-scale variations in DA and the flux power.

High-resolution spectrographs have the major advantage of allowing us to find and remove the individual Lyα lines of the LLSs and the metal lines in the Lyα forest. This reduces the sample size required for a given σ(DA) by about a factor of 4, and it greatly improves the accuracy of the corrections for the LLSs and metal lines. The factor of 4 largely compensates for the lower efficiency of high-resolution spectrographs in terms of photon recorded per Å per second. However, to find metal lines in high-resolution spectra we would prefer S/N > 10 per 0.03 Å, which is about 100 times more photons per Å than we have with Kast spectra. We would also require major

improvement in the flux calibration and continuum fits to the high-resolution spectra (Suzuki et al. 2003).

We could make the artificial spectra more similar to the Kast ones by reducing the absorption from the IGM, adding Lyα from LLSs and metals lines, and adding non-Gaussian errors to occasional pixels and flux calibration errors.

This work was funded in part by grant NAG5-13113 from NASA and by grant AST 00-98731 from the NSF. The spectra were obtained from the Lick observatory, and we thank the Lick Observatory staff. We are very grateful to Rupert Croft for drawing our attention to this topic and helping us understand the issues. We are especially grateful to Pat McDonald for providing us with the artificial absorption spectra and their description and for many detailed comments on the manuscript. We thank Joop Schaye for numerous thoughtful suggestions on the manuscript, especially his recommendation that we discuss the thermal history of the IGM. This research has made extensive use of the NASA/IPAC Extragalactic Database (NED), which is operated by JPL, under contract with NASA.

REFERENCES

Abel, T., & Haehnelt, M. G. 1999, ApJ, 520, L13
Abel, T., Norman, M. L., & Madau, P. 1999, ApJ, 523, 66
Bernardi, M., et al. 2003, AJ, 125, 32 (B0B)
Bi, H. G., Boerner, G., & Chu, Y. 1992, A&A, 266, 1
Bolton, J., Meiksin, A., & White, M. 2004, MNRAS, 348, L43
Bryan, G. L., & Machacek, M. 2000, ApJ, 534, 57
Burles, S. 1997, Ph.D. thesis, UCSD
Carswell, R. F., Whelan, J. A. J., Smith, M. G., Boksenberg, A., & Tytler, D. 1982, MNRAS, 198, 91
Cen, R., Nagamine, K., & Ostriker, J. P. 2004, preprint (astro-ph/0407143)
Ciardi, B., Ferrara, A., & White, S. D. M. 2003a, MNRAS, 344, L7
Ciardi, B., Stoehr, F., & White, S. D. M. 2003b, MNRAS, 343, 1101
Croft, R. A. C., Hernquist, L., Springel, V., Westover, M., & White, M. 2002a, ApJ, 580, 634
Croft, R. A. C., Weinberg, D. H., Bolte, M., Burles, S., Hernquist, L., Katz, N., Kirkman, D., & Tytler, D. 2002b, ApJ, 581, 20
Davé, R., Hernquist, L., Katz, N., & Weinberg, D. H. 1999, ApJ, 511, 521
Eisenstein, D. J., & Hu, W. 1999, ApJ, 511, 5
Fang, Y., Fan, X., Tytler, D., & Crotts, A. P. S. 1998, ApJ, 497, 67
Gardner, J., Katz, N., Hernquist, L., & Weinberg, D. 2003, ApJ, 587, 1
Gnedin, N. Y., & Abel, T. 2001, NewA, 6, 437
Gnedin, N. Y., & Hamilton, A. J. S. 2002, MNRAS, 334, 107
Haardt, F., & Madau, P. 1996, ApJ, 461, 20
Haehnelt, M. G., Madau, P., Kudritzki, R., & Haardt, F. 2001, ApJ, 549, L151
Hu, E. M., Kim, T., Cowie, L. L., Songaila, A., & Rauch, M. 1995, AJ, 110, 1526
Hui, L., & Haiman, Z. 2003, ApJ, 596, 9
Hui, L., Haiman, Z., Zaldarriaga, M., & Alexander, T. 2002, ApJ, 564, 525
Hui, L., & Rutledge, R. E. 1999, ApJ, 517, 541
Jenkins, E. B., & Ostriker, J. P. 1991, ApJ, 376, 33
Kim, T. S., Carswell, R. F., Cristiani, S., D'Odorico, S., & Giallongo, E. 2002, MNRAS, 335, 555
Kim, T.-S., Cristiani, S., & D'Odorico, S. 2001, A&A, 373, 757 (KCD01)
Kim, T.-S., Viel, M., Haehnelt, M. G., Carswell, R. F., & Cristiani, S. 2004, MNRAS, 347, 355
Kirkman, D., & Tytler, D. 1997, ApJ, 484, 672
Kirkman, D., Tytler, D., Suzuki, N., O'Meara, J. M., & Lubin, D. 2003, ApJS, 149, 1
Kolb, E. W., & Turner, M. S. 1990, The Early Universe (Reading: Addison-Wesley)
Liske, J., & Williger, G. M. 2001, MNRAS, 328, 653
Madau, P., Haardt, F., & Rees, M. J. 1999, ApJ, 514, 648
McDonald, P. 2003, ApJ, 585, 34
McDonald, P., Miralda-Escudé, J., Rauch, M., Sargent, W. L. W., Barlow, T. A., & Cen, R. 2001, ApJ, 562, 52
McDonald, P., Miralda-Escudé, J., Rauch, M., Sargent, W. L. W., Barlow, T. A., Cen, R., & Ostriker, J. P. 2000, ApJ, 543, 1
Meiksin, A., Bryan, G., & Machacek, M. 2001, MNRAS, 327, 296
Meiksin, A., & White, M. 2004, MNRAS, 350, 1107 (MW04)
Miralda-Escudé, J., & Rees, M. 1994, MNRAS, 266, 343
Misawa, T., Tytler, D., Iye, M., Storrie-Lombardi, L. J., Suzuki, N., & Wolfe, A. M. 2002, AJ, 123, 1847
Nakamoto, T., Umemura, M., & Susa, H. 2001, MNRAS, 321, 593
Norman, M. L., & Bryan, G. L. 1999, in Numerical Astrophysics, ed. S. M. Miyama & K. Tomisaka (Dordrecht: Kluwer), 19
Oke, J. B., & Korycansky, D. G. 1982, ApJ, 255, 11
Peterson, B. A. 1978, in IAU Symp. 79, Large-Scale Structures in the Universe, ed. M. S. Longair & J. EInasto (Dordrecht: Reidel), 389
Press, W., Rybicki, G., & Schneider, D. 1993, ApJ, 414, 64 (PRS93)
Rauch, M. 1998, ARA&A, 36, 267
Rauch, M., et al. 1997, ApJ, 489, 7
Razoumov, A. O., Norman, M. L., Abel, T., & Scott, D. 2002, ApJ, 572, 695
Sargent, W. L. W., Boksenberg, A., & Steidel, C. C. 1988, ApJS, 68, 539 (SBS88)
Sargent, W., Young, P., Boksenberg, A., & Tytler, D. 1980, ApJS, 42, 41
Schachter, J. 1991, PASP, 103, 457
Schaye, J., Aguirre, A., Kim, T.-S., Theuns, T., Rauch, M., & Sargent, W. L. W. 2003, ApJ, 596, 768
Schaye, J., Theuns, T., Leonard, A., & Efstathiou, G. 1999, MNRAS, 310, 57
Schaye, J., Theuns, T., Rauch, M., Efstathiou, G., & Sargent, W. L. W. 2000, MNRAS, 318, 817
Schneider, D. P., Schmidt, M., & Gunn, J. E. 1991, AJ, 101, 2004
Scott, J., Bechtold, J., & Dobrzycki, A. 2000, ApJS, 130, 37
Scott, J., Bechtold, J., Morita, M., Dobrzycki, A., & Kulkarni, V. P. 2002, ApJ, 571, 665
Scott, J., Kriss, G., Brotherton, M., Green, R., Hutchings, J., Shull, J., & Zheng, W. 2004, in ASP Conf. Ser. 311, AGN Physics with the Sloan Digital Sky Survey, ed. G. T. Richards & P. B. Hall (San Francisco: ASP), 31
Seljak, U., McDonald, P., & Makarov, A. 2003, MNRAS, 342, L79
Sokasian, A., Abel, T., & Hernquist, L. E. 2001, NewA, 6, 359
———. 2002, MNRAS, 332, 601
———. 2003a, MNRAS, 340, 473
Sokasian, A., Abel, T., Hernquist, L., & Springel, V. 2003b, MNRAS, 344, 607
Spergel, D. N., et al. 2003, ApJS, 148, 175
Steidel, C. C. 1990, ApJS, 72, 1
Steidel, C. C., Pettini, M., & Adelberger, K. L. 2001, ApJ, 546, 665
Steidel, C. C., & Sargent, W. L. W. 1987, ApJ, 313, 171 (SS87)
Stengler-Larrea, E. A., et al. 1995, ApJ, 444, 64
Storrie-Lombardi, L. J., & Wolfe, A. M. 2000, ApJ, 543, 552
Suzuki, N., Tytler, D., Kirkman, D., O'Meara, J. M., & Lubin, D. 2003, PASP, 115, 1050
———. 2004, ApJ, in press
Telfer, R. C., Zheng, W., Kriss, G. A., & Davidsen, A. F. 2002, ApJ, 565, 773
Theuns, T., Bernardi, M., Frieman, J., Hewett, P., Schaye, J., Sheth, R. K., & Subbarao, M. 2002, ApJ, 574, L111
Theuns, T., Leonard, A., & Efstathiou, G. 1998, MNRAS, 297, L49
Theuns, T., Leonard, A., Schaye, J., & Efstathiou, G. 1999, MNRAS, 303, L58
Theuns, T., Schaye, J., & Haehnelt, M. G. 2000, MNRAS, 315, 600
Tytler, D. 1982, Nature, 298, 427
———. 1987, ApJ, 321, 69
Tytler, D., O'Meara, J., Suzuki, N., Kirkman, D., Lubin, D., & Orin, A. 2004, AJ, 128, 1058
Valageas, P., Schaeffer, R., & Silk, J. 2002, A&A, 388, 741
Vanden Berk, D. E., et al. 2001, AJ, 122, 549
Viel, M., Haehnelt, M., & Springel, V. 2004, MNRAS, submitted (astro-ph/0404600)
Weinberg, D. H., Miralda-Escude, J., Hernquist, L., & Katz, N. 1997, ApJ, 490, 564
Wolfe, A. M., Turnshek, D. A., Smith, H. E., & Cohen, R. D. 1986, ApJS, 61, 249
Zaldarriaga, M., Scoccimarro, R., & Hui, L. 2003, ApJ, 590, 1
Zhang, Y., Anninos, P., Norman, M. L., & Meiksin, A. 1997, ApJ, 485, 496
Zhang, Y., Meiksin, A., Anninos, P., & Norman, M. L. 1998, ApJ, 495, 63
Zheng, W., Kriss, G. A., Telfer, R. C., Grimes, J. P., & Davidsen, A. F. 1997, ApJ, 475, 469